

MASTER THESIS

The uncertainty of discharge measurements and the water balance at river bifurcations



16 May 2022

Hide Wevers

University of Twente
Faculty of Engineering Technology
Department of Water Engineering and Management

Graduation committee

Dr. J.J. Warmink
Dr. V. Kitsikoudis
Dr. F. Huthoff

Preface

This thesis was written as part of my graduation for the Master Civil Engineering and Management at the University of Twente with a specialisation in River and Coastal Engineering. This research was conducted from November 2021 until May 2022 under the supervision of Jord Warmink, Vasilis Kitsikoudis and Freek Huthoff.

Although I did the research mainly at home, which was not always easy, I learned a lot during this process. I would like to thank Vasilis for his active guidance and support, weekly meetings, and fast and detailed feedback on my questions during this process. I would also like to thank Freek for giving me very useful feedback to get to the core of the problem and providing me with the ADCP dataset. Furthermore, I would like to thank Jord for the detailed feedback and taking care of general matters.

I hope you enjoy reading.

Hidde Wevers

Enschede, 16 May 2022

Summary

Discharge time series are mainly derived from rating curves using continuously measured water levels. Rating curves rely on periodic discharge and water level measurements. In the Netherlands, periodic discharge measurements are regularly performed during high discharge events often using the moving-boat Acoustic Doppler Current Profiler (ADCP) method. However, not every part of the river cross-section can be measured with an ADCP measuring instrument, which is often located near the water surface, the bed, the banks and at inundated floodplains. The discharge in these unmeasured zones must be estimated by extrapolation of the available ADCP measurements and this introduces uncertainty in the total discharge measurement, which directly translates into uncertainty in rating curves and the derived discharge data. Therefore, accurate discharge measurements are essential for flood risk management in the Dutch river area, especially during extreme events.

This research focuses on the river branches at the Pannerdensche Kop, which is the bifurcation of the Bovenrijn in the Waal and the Pannerdensch Kanaal. Currently, rating curves as well as the underlying discharge data do not show a closing water balance at the Pannerdensche Kop. This is a direct indication of errors in the rating curves, which are partly due to uncertainties in the periodic discharge measurements. Therefore, the main aim of this research is to quantify the uncertainty of high discharge measurements and its influence on the water balance at the Pannerdensche Kop.

Firstly, the uncertainties introduced in the discharge measurements are quantified and propagated to the overall uncertainty. The overall uncertainty is subdivided into the random uncertainty, edge uncertainty, extrapolation uncertainty, velocity uncertainty, bottom depth uncertainty and systematic uncertainty. Of the uncertainties, only the random and systematic uncertainty have a significant influence on the overall uncertainty. The systematic uncertainty is assumed constant for each measurement and the random uncertainty depends on the coefficient of variation of the total discharge for all transects and the number of transects. The overall uncertainties in the Bovenrijn are fairly constant over all measurements, ranging from 3.09% to 5.25%. In the Waal, there are larger fluctuations in the overall uncertainty over time from 3.66% to 9.75%. However, the largest uncertainties are probably overestimated compared to the lowest uncertainties due to a negative correlation with the number of transects. The Pannerdensch Kanaal has relatively large uncertainties over time, ranging from 3.74% to 9.90%.

Secondly, the uncertainty was also estimated for all discharge components (i.e., edges, floodplains, top and bottom unmeasured zones and measured zone) individually. Although the measured discharge has the lowest degree of uncertainty, it has the greatest influence on the overall uncertainty as its discharge is responsible for a large fraction of the total discharge. After that, the top and bottom discharges account for the second and third largest fraction of total discharge but also have the second and third smallest degree of uncertainty. As a result, the fully inundated floodplains have a larger influence on the overall uncertainty. Although surrounded by uncertainty, the edge discharges generally have a small influence on the overall uncertainty.

Finally, the comparison between the estimated ADCP discharges and the historical derived discharges showed no systematic over- or underestimation of the discharge by the rating curves for any of the branches. However, three ADCP measurements are slightly over- and underestimated by the rating curve, but this can be partly explained by the time delay in the discharge between the station and the ADCP measurement location. Additionally, it was found that by including the uncertainties in the river branches into the water balance error, the perfect water balance closure falls within the 95% confidence interval for all same-day ADCP measurements in the three branches. Therefore, the water balance error at the Pannerdensche Kop can be explained by the uncertainties in the three river branches and there seems to be no river branch that most likely caused the water balance error.

Table of Contents

| | |
|---|----|
| Preface..... | I |
| Summary | II |
| 1 Introduction..... | 5 |
| 1.1 Context | 5 |
| 1.2 Problem description | 6 |
| 1.3 Research aim and questions..... | 7 |
| 1.4 Study area..... | 7 |
| 2 Theoretical framework..... | 8 |
| 2.1 Periodic discharge measurements | 8 |
| 2.1.1 Standard velocity-area method..... | 8 |
| 2.1.2 Adjusted velocity-area methods | 9 |
| 2.2 Continuous discharge measurements..... | 11 |
| 2.3 Discharge time series derived from rating curves..... | 11 |
| 2.4 Limitations of the measuring instruments | 12 |
| 2.4.1 Boat-mounted ADCP | 12 |
| 2.4.2 ADM..... | 12 |
| 2.4.3 H-ADCP | 12 |
| 2.5 Summary..... | 12 |
| 3 Research methodology..... | 13 |
| 3.1 Data availability | 13 |
| 3.2 Data pre-processing | 13 |
| 3.3 Uncertainties in high river discharge measurements and their weight on the overall uncertainty | 14 |
| 3.3.1 Procedure to determine river discharges during high discharge events | 14 |
| 3.3.2 Possible uncertainties in the measuring procedure and weight of each uncertainty .. | 24 |
| 3.4 The uncertainty of the total discharges in the branches and the water balance of the Pannerdensche Kop..... | 26 |
| 4 Results | 29 |
| 4.1 Uncertainties in high river discharge measurements and their weight on the overall uncertainty | 29 |
| 4.1.1 Uncertainties in the measuring procedure and the weight of each uncertainty..... | 31 |
| 4.2 The uncertainty of the total discharges in the branches and the water balance of the Pannerdensche Kop..... | 37 |
| 5 Discussion..... | 40 |
| 5.1 Uncertainty propagation approach..... | 40 |

| | | |
|-----|---|----|
| 5.2 | ADCP error velocity | 40 |
| 5.3 | Flow inhomogeneity..... | 40 |
| 5.4 | Uncertainty in floodplain discharges..... | 41 |
| 6 | Conclusion | 42 |
| 6.1 | Uncertainties in high river discharge measurements and their weight on the overall uncertainty | 42 |
| 6.2 | The uncertainty of the total discharges in the branches and the water balance of the Pannerdensche Kop..... | 43 |
| 7 | Recommendations..... | 44 |
| | References..... | 45 |
| | Appendix A: Equations of extrapolation methods | 47 |
| | Appendix B: Figures | 48 |
| | Appendix C: Correlation analysis..... | 49 |

1 Introduction

1.1 Context

The Netherlands is known for its rich history in water management in order to control the risk of flooding. Flood risk management in the Netherlands nowadays depends largely on hydrodynamic models. The reliability of these models depends on the accuracy of discharge time series, as these time series are used in the calibration and validation of hydrodynamic models. Discharge time series are mainly derived from rating curves using measured water level time series, rather than measuring the discharges directly (Quartel et al., 2011). Rating curves indicate the relationship between river discharge and water level at a certain location in a river and are developed by fitting a curve to a limited number of discharge and water level measurements. In the Netherlands, rating curves are often applied since water level measurements can be performed more straightforwardly and accurately than discharge measurements. For example, rating curves are used for determining daily discharge data for both the Bovenrijn and the Waal (Buschman et al., 2017). Figure 1 shows an example of rating curves developed for three key locations along the Rhine. It can be seen that most measuring points originate from measurements performed under moderate flow conditions.

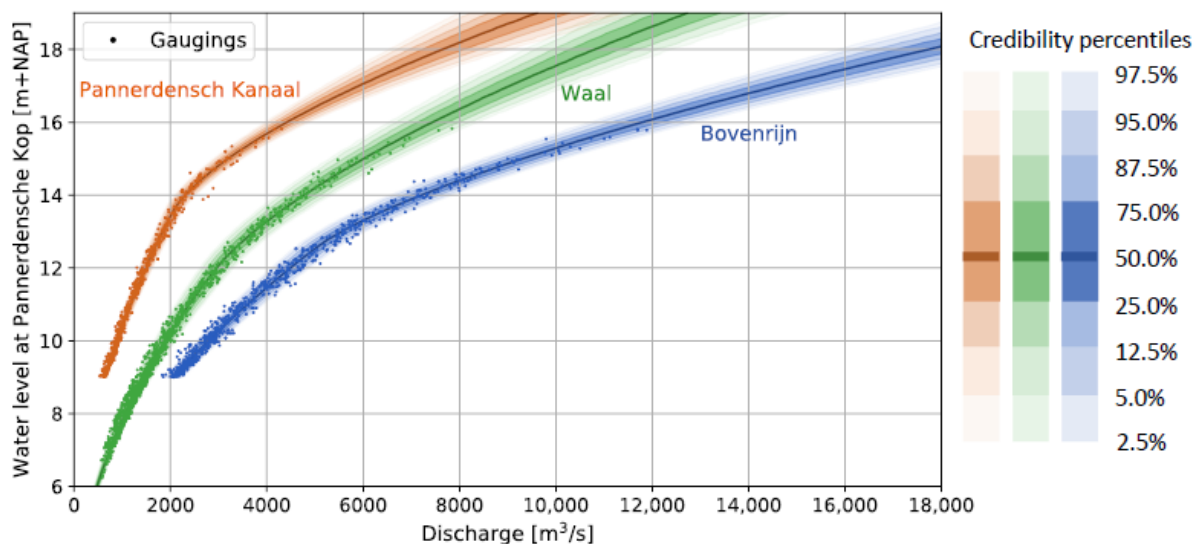


Figure 1: Example of rating curves for the Bovenrijn, the Pannerdensch Kanaal and the Waal near the Pannerdensch Kop together with paired measurement points (Gensen, 2021).

An Acoustic Doppler Current Profiler (ADCP) is an instrument based on measuring the Doppler shift of a transmitted acoustic wave reflected by the particles in the water, where the Doppler shift is the difference in the frequency of the reflected transmitted sound wave and thus a measure of the water velocity (Hartong & Termes, 2009). Together with measured cross-sectional areas, the measured water velocities are translated into discharges and referred to as discharge measurements. However, discharge time series are derived from continuously measured water levels through a rating curve. Therefore, there is a clear distinction between measured and derived discharges. Rating curves rely on periodic discharge measurements. These are regularly carried out by Rijkswaterstaat and supplemented by targeted measurement campaigns during high discharge events. The high discharge events are particularly important because they largely determine the shape of a fitted rating curve for estimating conditions of the most extreme events.

Fitting a rating curve for the most extreme events is performed by extrapolation, as discharge measurements are not available in the entire domain of observed extreme water levels. In simple cases, the curve may be smoothly extended. However, this is not accurate if, in the extended range, the river geometry changes, there is flow over the floodplains and the hydraulic roughness changes (Jain & Singh, 2003). This is all the case when floodplains are inundated, whose main function is to increase the discharge capacity of rivers during high water levels. As a result, inundated floodplains introduce uncertainty in the extreme discharge domain which directly translates into uncertainty in the derived discharge data. Therefore, to guarantee safety in the Dutch river area, accurate measurements of the discharge through the main channel and over the floodplains are essential, especially during extreme events.

1.2 Problem description

In the Netherlands, the moving-boat method is often used to perform periodic discharge measurements in a river, where water velocities are measured relatively quickly at constant depth from a boat using a boat-mounted ADCP (Hartong & Termes, 2009). However, not every part of the river cross-section can be measured. Unmeasured zones are often located near the water surface, the bed and the banks. The ADCP provides unreliable results near the bed due to side-lobe interference, causing errors in the measured Doppler shift, and near the water surface due to the draft and flow disturbance of the instrument and the required blanking distance (Mueller & Wagner, 2009). Therefore, the discharge in these unmeasured zones must be estimated by extrapolation or using some approximate models based on the collected data in the measured zone of the river cross-section and is thus surrounded by uncertainty (J. A. González-Castro & Muste, 2007; Mueller & Wagner, 2009).

In addition, with regard to performing high water level measurements with inundated floodplains, in many cases it is not possible to measure above the floodplains for practical reasons. It is too shallow for measuring boats to navigate over the floodplains. The actual measurement data therefore usually concerns the discharge in the main channel and only some parts of the floodplains. For the determination of water velocities in floodplains, estimates and assumptions of the fitted velocity profiles are made based on height profile measurements and hydraulic roughness measurements (Hartong & Termes, 2009). Using these estimates of water velocities and cross-sectional area in floodplains, the discharge in the floodplains is added to the discharge in the main channel.

Although the height profile of floodplains can be derived with a certain accuracy (± 7 cm) from aerial photographs, assumptions have to be made by the surveyor for the determination of the hydraulic roughness (Hartong & Termes, 2009). Furthermore, the flow pattern near the water surface is very sensitive to external influences such as the wind, where the velocity and direction of the flow can fluctuate (Hartong & Termes, 2009). Therefore, estimated floodplain discharges could introduce a large uncertainty in the total discharge measurements, which directly translates into uncertainty in the developed rating curves. As a result, design water levels, flood risks and the impacts of river interventions can be calculated with less accuracy.

Currently, rating curves as well as the underlying discharge data do not show a closing water balance over the Dutch Rhine branches (Twijnstra et al., 2020), i.e. the incoming discharge is not equal to the outgoing discharges at the Pannerdensche Kop. This is a direct indication of errors in the rating curves, which are partly due to uncertainties in the discharge measurements. The amount of discharge in a branch has a dominant influence on the water levels along the downstream branches. Accurate estimates of discharges are thus essential for river management purposes.

1.3 Research aim and questions

The main aim of this research is to quantify the uncertainty of discharge measurements during high discharge events and its influence on the water balance at river bifurcations.

The following research questions have been formulated:

1. Which uncertainties does the measuring procedure introduce in the final estimate of the total discharge and what is the weight of each uncertainty on the overall uncertainty?
2. Which rating curve of the branches at the Pannerdensche Kop is the most uncertain, due to the uncertainty in estimated discharge values, and most likely causes the water balance error?

1.4 Study area

The research focuses on the locations near the first major bifurcation in the Dutch Rhine River branches, i.e., upstream and downstream of the Pannerdensche Kop (see Figure 2). The Pannerdensche Kop is located near Pannerden and is the bifurcation of the Bovenrijn into the Pannerdensch Kanaal and the Waal. This study area is chosen since the Pannerdensche Kop in the river Rhine is of great significance for water management in the Netherlands.

The discharge distributions at the most important bifurcations of the Rhine, and thus the discharge in the downstream branches, have been calculated based on the design discharge at Lobith and are established in the River Engineering Assessment Framework (in Dutch: Rivierkundig Beoordelingskader) (Rijkswaterstaat Water Verkeer en Leefomgeving, 2019). At the Pannerdensche Kop, about 64% of the Rhine River water flows into the Waal and the other 36% flows into the Pannerdensch Kanaal at the design discharge of 16,000 m³/s at Lobith (Rijkswaterstaat Water, Verkeer en Leefomgeving, 2019). This discharge distribution has a dominant influence on the water levels across the downstream branches and a constant discharge distribution is therefore desirable. Conversely, changes in water levels in the downstream branches of the Pannerdensche Kop can affect the discharge distribution at the bifurcation point due to backwater effects.

Rating curves have been constructed for eight locations in the Dutch Rhine system, including the locations directly downstream of the Pannerdensche Kop (i.e. the Pannerdensch Kanaal and the Waal) and upstream of the Pannerdensche Kop near Lobith, close to where the Rhine enters the Netherlands (Hartong & Termes, 2009).

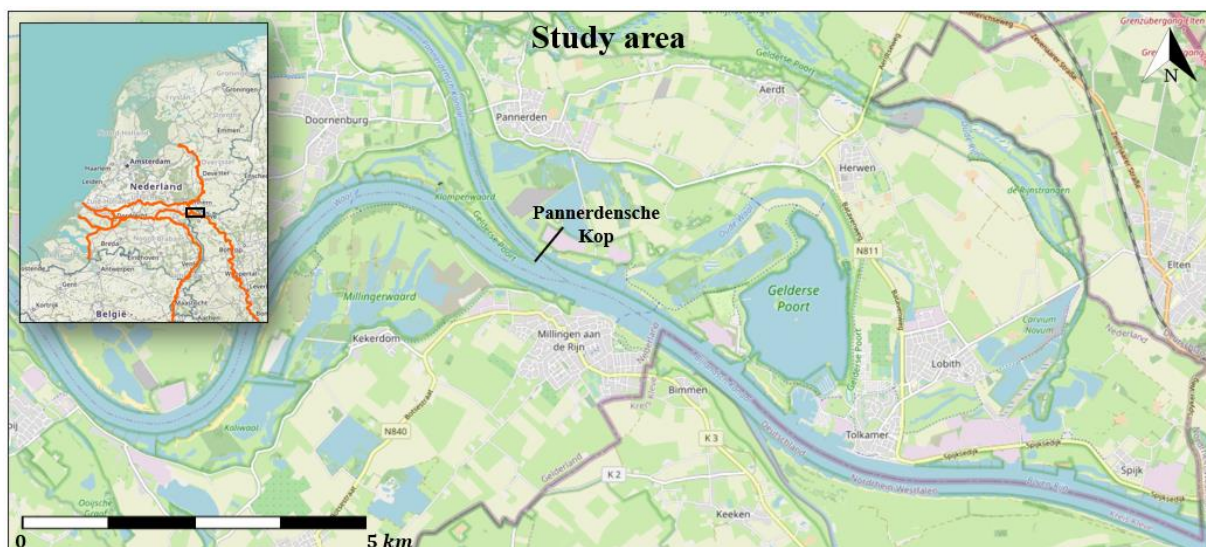


Figure 2: Map of the Pannerdensche Kop bifurcation.

2 Theoretical framework

Discharge measurements have been carried out in the Netherlands for many years. From 1901, continuous discharge measurements of the Rhine started on a daily basis (Buschman et al., 2017). Measuring technology has evolved significantly over the years.

For carrying out discharge measurements nowadays, the Stichting Toegepast Onderzoek Waterbeheer (STOWA) has established a handbook for measuring river discharges in open waterways (Hartong & Termes, 2009). This handbook describes in great detail how water managers should measure river discharges in the Netherlands. Measurement techniques and methods that are relevant to this research will be explained in more detail in the theoretical framework.

A distinction must be made in the frequency (periodic or continuous) of the measurements and the associated measuring techniques and methods. Periodic and continuous measurements have different purposes and different measuring techniques and methods are used for this.

2.1 Periodic discharge measurements

From the period 1988 to 2004, periodic discharge measurements were performed using helical Ott-mills (mechanical hydrometric current meters) (Buschman et al., 2017). However, since 2002, river discharges have been established using Acoustic Doppler Current Profilers (ADCP), an instrument that measures water velocities based on the Doppler effect and which can be converted into discharges by the surveyor.

2.1.1 Standard velocity-area method

Measuring discharges essentially comes down to the basic principle of $Q = V \cdot A$. In which A is the area of a river with arbitrary cross-section and V is the flow velocity over the cross-section. Here, the depth-averaged flow velocity and the cross-sectional area for several locations in a river section are measured and multiplied with each other. Summed up, this results in the total discharge Q at the location of measuring. So more accurately, the basic principle can be written as $Q = \sum(V_i \cdot A_i)$ where i indicates the location in the river cross-section. The area of the cross-section is calculated from the measured width of the river section and some depth soundings. The depth is measured in a number of verticals.

This method is based on steady flow in a free water surface. Due to bed friction, the flow velocity near the bottom and the banks of a river is lower than the average flow velocity. For the velocity profile of a turbulent steady and uniform flow a general logarithmic or power velocity profile in both the vertical and horizontal plane is often assumed (Hartong & Termes, 2009). The average flow velocity in each vertical can be determined based on an assumption of the velocity profile.

There are several methods to determine the total discharge based on the calculated cross-sectional areas of the river and the associated depth-averaged flow velocities. Common methods are the mean-section method and the mid-section method (Hartong & Termes, 2009). In the mean-section method, the entire cross-section is divided into segments, the total discharge is then calculated as the sum of the discharges of the individual segments. In this method, a flow velocity reduction is assumed near the banks and this can be applied if the banks are free of vegetation. In the mid-section method, the cross-section is also divided into segments, but the bank segments are excluded. It is assumed that there is no discharge here and is applied in case of vegetated banks. As with the mean-section method, the total discharge is calculated by the summation of the individual discharges.

However, the standard velocity-area method also has its limitations. The method is generally not very suitable for unsteady flow conditions, wide rivers, shipping traffic and inundated floodplains (Hartong & Termes, 2009).

2.1.2 Adjusted velocity-area methods

To cope with the limitations of the standard velocity-area method, the method was adjusted. In the Netherlands, the moving-boat method is often used for this, where flow measurements are performed relatively quickly using a boat-mounted ADCP (Figure 3).

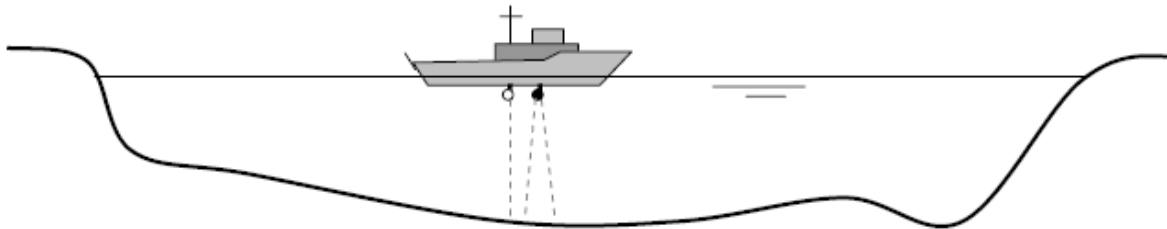


Figure 3: A visualisation of the moving-boat ADCP method (Hartong & Termes, 2009).

The ADCP continuously measures water velocity vectors (\vec{V}_w) and boat velocity vectors (\vec{V}_b) over the river cross-section for a number of vertical profiles (see Figure 4). The discrete segments of the vertical profile are referred to as bins or depth-cells, whereas the collection of depth-cells in a single vertical profile is referred to as an ensemble (Moore et al., 2017). The water velocity is computed as the product of the water velocity magnitude $|\vec{V}_w|$ and sine of the internal angle θ of the water velocity vector and the boat velocity vector (Mueller & Wagner, 2009; TRDI, 2016):

$$V = |\vec{V}_w| \cdot \sin \theta \quad (1)$$

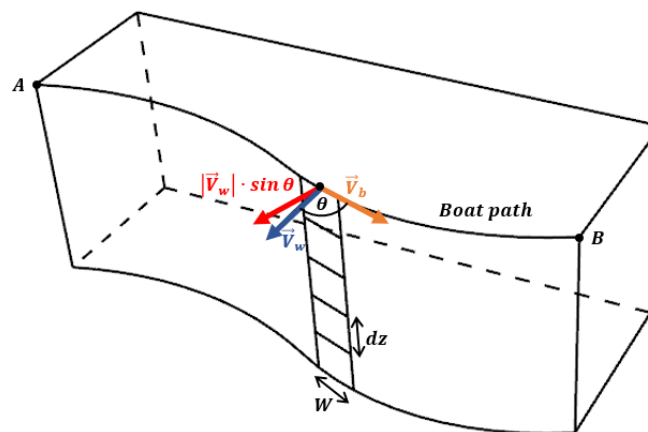


Figure 4: Definition sketch with boat and water velocity vectors for a single depth-cell in an ADCP ensemble. Adapted from (Mueller & Wagner, 2009).

Although the boat tends to navigate at a constant speed, the exact navigation speed relative to the riverbed still needs to be determined. Different references can be used for this. Firstly, the ADCP measures its displacement relative to the detected fixed bed, this is called bottom-track. Secondly, the measured water velocities can be combined with the boat's displacement measured with independent GPS. At high river flows, the riverbed can be set into motion parallel to the direction of the flow due to the pressure variations exerted on the bed. This mainly occurs in situations with the presence of a loose, water-saturated top layer on the bed (fluid mud layer) (Eij, 2004). Due to the moving riverbed, the ADCP cannot accurately perform the reference measurement using bottom-track. The water

velocities are then measured relative to the bed moving with the flow so they will be biased in the direction of the flow. Measurements during a moving riverbed can be corrected by comparison with independent GPS data (Eij, 2004).

The water velocities in the unmeasured zones; located near the water surface, the bed and the banks; are often estimated by extrapolation of the available ADCP measurements in ADCP software (Hartong & Termes, 2009; Mueller & Wagner, 2009), see Figure 5. There are three commonly used methods for estimating the top discharge (J. A. González-Castro & Muste, 2007; Mueller & Wagner, 2009; TRDI, 2016):

1. Fitting a power law or logarithmic distribution to the velocity profile in the water column;
2. Applying the constant extrapolation method: the water velocity in the top measured depth-cell is a good estimate for the average water velocity in the top unmeasured zone;
3. Applying the 3-point slope method: the slope of the vertical velocity profile follows the slope of the three top measured depth-cells.

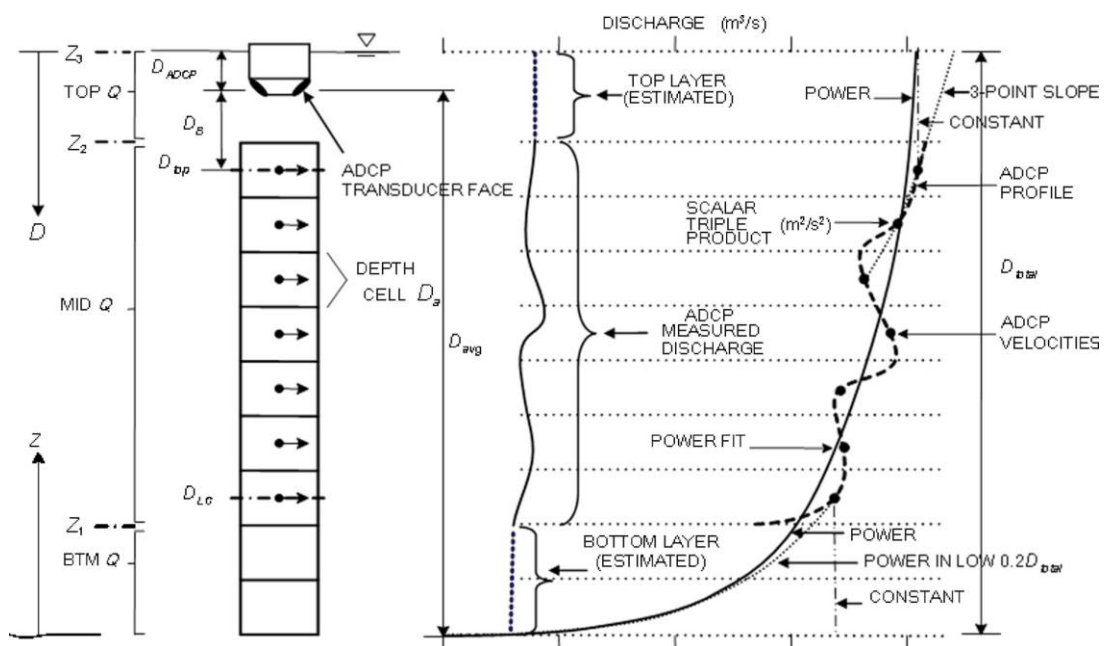


Figure 5: Overview of different methods to estimate the discharge in the top and bottom unmeasured zones based on assuming a velocity profile (González-Castro & Muste, 2007).

Due to bed friction, the water velocity near the bed is lower than the velocity in other parts of the water column. Two commonly used methods for estimating the bottom discharge are (J. A. González-Castro & Muste, 2007; Mueller & Wagner, 2009; TRDI, 2016):

1. Fitting a power law or logarithmic distribution to the velocity profile in the entire water column where the no-slip condition applies at the bed;
2. Fitting a power law distribution to the velocity profile in only the bottom 20% of the water column where the no-slip condition applies at the bed. When there are no flow measurements in the lowest 20% of the water column, the power distribution parameters can be estimated based on the measured velocity in the lowest measured depth-cell.

The water velocities in the measured zones are converted to discharges by integration over the measured depth-cells (bins) (Hartong & Termes, 2009; Mueller & Wagner, 2009). The integration process is based on the basic principle of $Q = \bar{V} \cdot A$. Where \bar{V} is the mean water velocity perpendicular to the cross-sectional area A . The periodic discharge measurements often serve as calibration and validation for the fixed continuous discharge measuring stations, since only a part of the river cross-section can be measured with a fixed measuring station (Brand, 2011). Periodic discharge measurements are also carried out during high water conditions in places where no continuous measuring stations are installed to gain more insight into the behaviour of river discharge during high water (Buschman et al., 2017).

2.2 Continuous discharge measurements

With continuous measurements, the river discharge is measured at a fixed location over a longer period with a frequency in the order of magnitude of an hour. Nowadays, possible instruments for performing continuous discharge measurements are (Hartong & Termes, 2009):

- Acoustic Discharge Meters (ADM),
- Horizontal Acoustic Doppler Current Profilers (H-ADCP),

The ADM is based on the principle of accurately measuring the transit times of transmitted acoustic signals in the water within a measuring section, from which the flow velocities can be calculated. The measured flow velocities are translated into an average flow velocity over the cross-section by multiplication with a correction factor K . The discharge is then determined by multiplying the obtained average flow velocity over the cross-section by the area of the cross-section. The area is determined by measuring a number of cross-sections in the measuring section and taking the average.

The horizontal ADCP is installed on one side of the river and is facing the cross-section transversely. The H-ADCP is based on measuring the Doppler shift of a transmitted acoustic wave reflected by the particles in the water. The Doppler shift is the difference in the frequency of the reflected transmitted sound wave and thus a measure of the velocity of the water. The water level is also measured by the H-ADCP technique and converted to a cross-sectional area according to a pre-constructed water level-cross-sectional area relationship. Subsequently, the total discharge can be calculated by multiplying the area of a river cross-section with the water velocity over the cross-section.

2.3 Discharge time series derived from rating curves

Water levels are measured relative to Amsterdam Ordnance Datum (NAP) by automatic float-driven shaft encoders (Berends, 2019). In open waterways, there is a more or less unambiguous relationship between water level and discharge, also called rating curves (Hartong & Termes, 2009). Rating curves are determined by fitting a curve through a limited number of discharge and water level measurements. High-quality rating curves are fundamental for the application of discharge time series in hydrodynamic models such as SOBEK and WAQUA and in flood forecasting. The advantage of rating curves is that it allows continuous discharge time series to be determined without requiring continuous discharge measurements. A disadvantage is that the uncertainty of the derived discharge increases in the extremely high water regime, as there are few direct discharge measurements in this regime.

However, studies show that the standard rating curves are insufficiently accurate since no temporal variations are incorporated in the equation (Hartong & Termes, 2009). Deviations between the measured and derived discharges can occur due to morphological changes of the riverbed (degradation or sedimentation), changes in hydraulic roughness (vegetation and bedforms), weir effects and flood waves. Flood waves lead to a change in the hydraulic gradient with the result that

the discharge is higher at rising water and lower at falling water (hysteresis) than is derived from the established rating curve (Hartong & Termes, 2009).

2.4 Limitations of the measuring instruments

2.4.1 Boat-mounted ADCP

A disadvantage of a boat-mounted ADCP is that it cannot measure water velocities near the riverbed and the water surface. The ADCP provides unreliable results near the bed due to side-lobe interference and near the water surface due to the draft of the instrument and the required blanking distance (Mueller & Wagner, 2009).

2.4.2 ADM

Disadvantages of an ADM are that its transmitters, receivers and cables need maintenance and that the hydraulic roughness and cross-sectional area must be accurately known and adjusted in case of changing conditions. In addition, installing an ADM involves high initial costs. And finally, the ADM is sensitive to large amounts of sediment that is released during high water. However, the big advantage is that an ADM produces a robust width-averaged flow velocity, which can also be used to determine the discharge during low and high river discharges (Buschman et al., 2017).

2.4.3 H-ADCP

A horizontal ADCP is a worldwide accepted method for measuring continuous water velocities, from which discharges are calculated. An advantage over an ADM is that with an H-ADCP only one location needs to be maintained and no cables need to be laid under the riverbed. However, as soon as there is floodplain flow, the H-ADCP cannot provide accurate continuous discharge measurements anymore due to underestimation at high discharges (Hartong & Termes, 2009).

2.5 Summary

The handbook by Hartong & Termes (2009) describes a wide range of methods and techniques to measure river discharges in the Netherlands. However, the technical background of the method to convert boat-mounted ADCP flow measurements to discharges is not described in great detail here, while the measurements in the provided dataset in this research were performed using this measuring instrument (see Section 3.1)

In contrast, Mueller & Wagner (2009) and González-Castro & Muste (2007) provide methods to convert ADCP flow measurements to discharges in the measured zone and methods to estimate the discharge in the unmeasured zones of a river cross-section based on the available flow measurements. The estimation methods are based on extrapolation techniques and approximate models that are often already part of an algorithm that can be implemented in various ADCP software, however, the use of ADCP software is outside the scope of this research. Instead, the provided boat-mounted ADCP flow measurements will be converted to the total discharge by implementing and applying the equations, extrapolation techniques and approximate models of Mueller & Wagner (2009) and González-Castro & Muste (2007) in MATLAB. This process is described in more detail in the Section 3.

3 Research methodology

3.1 Data availability

A dataset with flow measurements performed with a boat-mounted ADCP in the period from 3 to 11 November 1998 during a high-discharge event is provided. The measurements were carried out by Rijkswaterstaat up- and downstream of the Pannerdensche Kop and processed by the external party Aqua Vision (Eij, 2004), see Table 1 for an overview. During the measurement campaign, two measurement ships were used, the M.S. Rasse and the M.S. Ponderosa. Both ships were equipped with an RD Instruments ADCP 1200 kHz BroadBand, GPS navigation system Sercel 103 and gyrocompass.

Table 1: Overview of measured locations with name, chainage, ship and measurement period (Eij, 2004).

| Name | Location | Chainage [km] | Ship | Dates |
|------|---------------------|------------------|------------|-------------------------|
| BR | Bovenrijn | 863.9 | M.S. Rasse | 3-6, 9-11 November 1998 |
| WAA | Waal | 870.5 | | 3-6, 9-11 November 1998 |
| PK | Pannerdensch Kanaal | 869.0 | | 4-6, 9-11 November 1998 |

The provided dataset only contains the corrected ADCP measurements which were converted to ASCII files, consisting of the measurement data listed in Table 2. The raw ADCP data is not available.

Table 2: Name, description and unit of the provided ADCP measurement data (Eij, 2004).

| Name | Description | Unit |
|---------------------|---|------------|
| East Displacement | x -coordinate of the boat-mounted ADCP | m |
| North Displacement | y -coordinate of the boat-mounted ADCP | m |
| Z | z -coordinate of depth-cells relative to the water surface | m |
| Date | Date of measurement | YYYY-MM-DD |
| Time | Time of measurement | hh:mm:ss |
| Depth | depth of bed relative to the water surface | m |
| East Velocity | East component of the water velocity vector | m/s |
| North Velocity | North component of the water velocity vector | m/s |
| Velocity Magnitude | Magnitude of the water velocity vector | m/s |
| Velocity Direction | Direction of water velocity vector clockwise with respect to North | ° |
| ADCP Error Velocity | Difference between two vertical velocity components of two pair of acoustic beams | m/s |

The ADCP measurement data are expressed in the Earth coordinate system RDV based on the default bottom-track navigational reference system and in case of a moving riverbed, independent GPS navigational reference system.

3.2 Data pre-processing

As already mentioned, raw ADCP data from 1998 has been pre-processed by Aqua Vision and converted into corrected ASCII files. The pre-processing of the raw ADCP data consists of the following steps (Eij, 2004):

1. Incomplete and unusable navigated transects have been removed from the dataset.
2. Depth-cells and ensembles with unrealistic deviations in water velocities and echo intensities were removed and replaced by horizontal linear interpolation with neighbouring values.

3. Optimisation of raw navigation data (GPS) of the M.S. Rasse by correcting for time delay and deviating position with respect to the ADCP, based on the boat velocity vectors from the bottom-track navigational reference system.
4. Correcting the compass deviation in the measurements with the M.S. Ponderosa by comparing bottom-track navigation path with the GPS navigation path.
5. Transects where a moving riverbed has occurred, indirectly leading to an underestimation of the water velocities, have been corrected by replacing the bottom-track navigational reference system with the independent GPS navigational reference system of the boat displacement.

The corrected ASCII files are imported and processed in MATLAB for computing the discharge from the ADCP flow measurements.

3.3 Uncertainties in high river discharge measurements and their weight on the overall uncertainty

To answer the first research question, the procedure for determining river discharges during high discharge events was first analysed. During the measurement procedure, assumptions and estimates were made that lead to uncertainty in the calculated total discharge. These assumptions were made explicit and quantified and then propagated to the overall uncertainty in the estimated discharge for each location.

3.3.1 Procedure to determine river discharges during high discharge events

ADCP flow measurements were obtained along cross-sections at the Bovenrijn, the Waal and the Pannerdensch Kanaal over the periods 3 to 6 and 9 to 11 November 1998. The measurement boat followed a number of transects each day along a predetermined navigational transect where the depth and water velocities were measured for each transect at a large number of points. All navigated transects at the Pannerdensche Kop over the entire measurement period are shown in Figure 6.

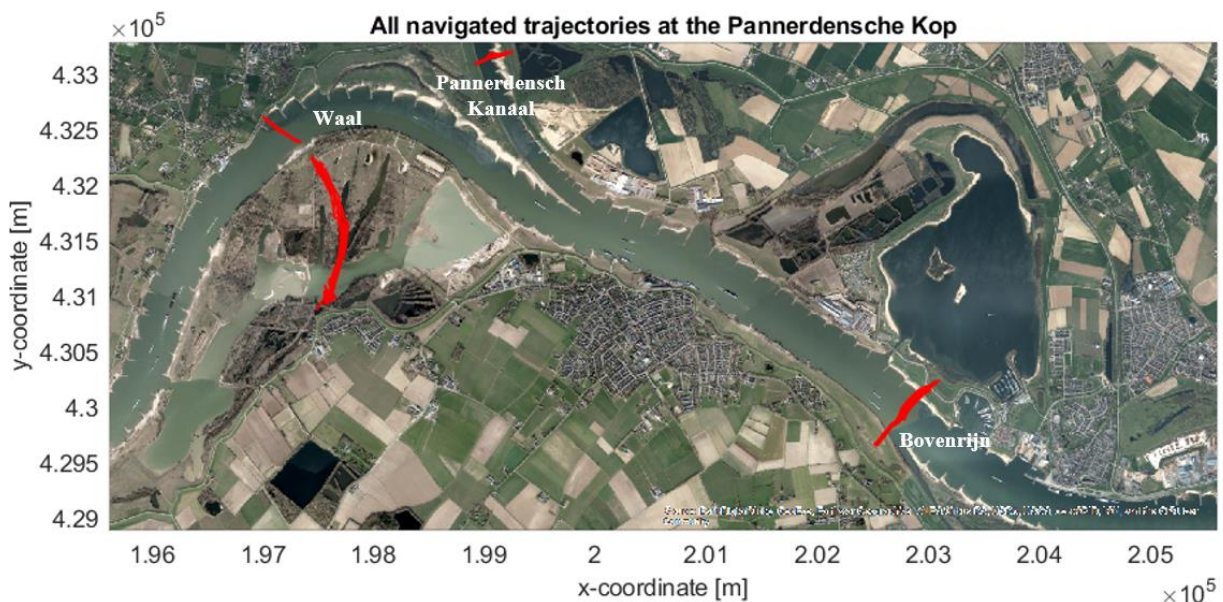


Figure 6: The navigated transects over the measurement period at all river branches at the Pannerdensche Kop.

Figure 7 shows that water velocity measurements are missing in certain parts of the cross-sections since the ADCP is not able to measure the water velocities over the entire water column. The water velocities were measured between 1.32 m below the water surface for all river branches to

approximately 60 cm above the riverbeds with a constant depth interval (or depth-cell size) of 25 cm. The average horizontal distance between the ensembles is 4 m.

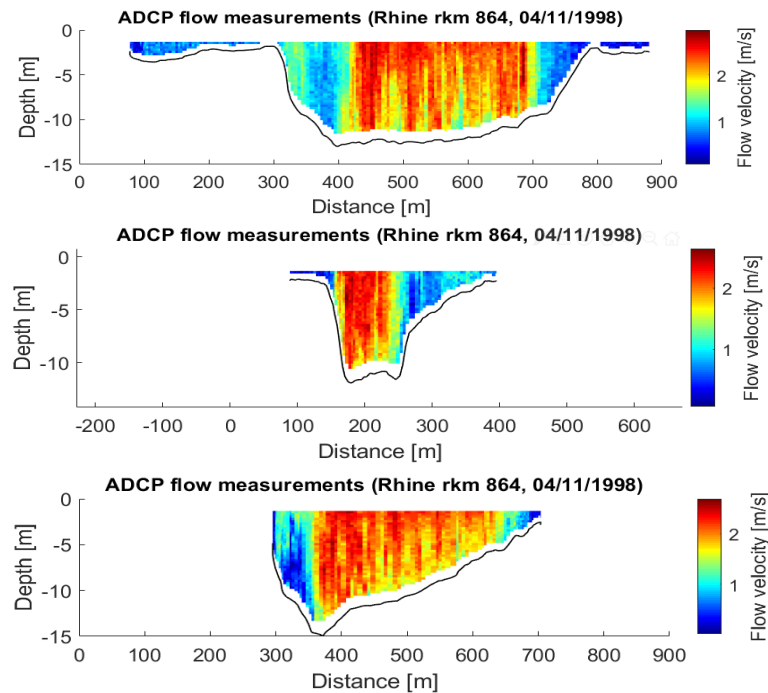


Figure 7: ADCP flow measurements over the river cross-section for arbitrary transects at the Bovenrijn (upper), the Waal (centre) and the Pannerdensch Kanaal (bottom) on 4 November 1998.

The water velocities in the unmeasured zones are determined by extrapolation of the available ADCP measurements. Therefore, the total discharge of the river cross-section is calculated by the summation of the calculated discharge in the measured zones and the extrapolated estimates of the discharge in the unmeasured zones. The process of computing the total discharge from ADCP flow measurements will be performed in MATLAB and the mathematical background of this process will be described below.

The equation for calculating the total discharge (Q_{tot}) for one navigated transect is based on (J. A. González-Castro & Muste, 2007; Mueller & Wagner, 2009) (see Figure 8) and written as follows:

$$Q_{tot} = Q_{left} + Q_{fp_{left}} + Q_{top} + Q_m + Q_{m,est} + Q_{bottom} + Q_{fp_{right}} + Q_{right} \quad (2)$$

Where,

- Q_{left} = estimated discharge for segment near left bank [m^3/s]
- $Q_{fp_{left}}$ = estimated discharge through left floodplain [m^3/s]
- Q_{top} = estimated discharge for top unmeasured zone of main channel [m^3/s]
- Q_m = computed discharge from ADCP flow measurements in main channel [m^3/s]
- $Q_{m,est}$ = estimated discharge for missing or invalid cells of measured zone [m^3/s]
- Q_{bottom} = estimated discharge for bottom unmeasured zone of main channel [m^3/s]
- $Q_{fp_{right}}$ = estimated discharge through right floodplain [m^3/s]
- Q_{right} = estimated discharge for segment near right bank [m^3/s]

The final discharge in an ADCP measurement is the average of a number of M single-transect discharges from successive crossings of the river, under approximately steady flow conditions. The average should include pairs of reciprocal transects to minimise any potential directional biases in measured discharges, due to asymmetrical deployment, compass, or heading errors (Mueller & Wagner, 2009).

The different discharge components leading to the total discharge in Equation (2) are schematised in the river cross-section in Figure 8.

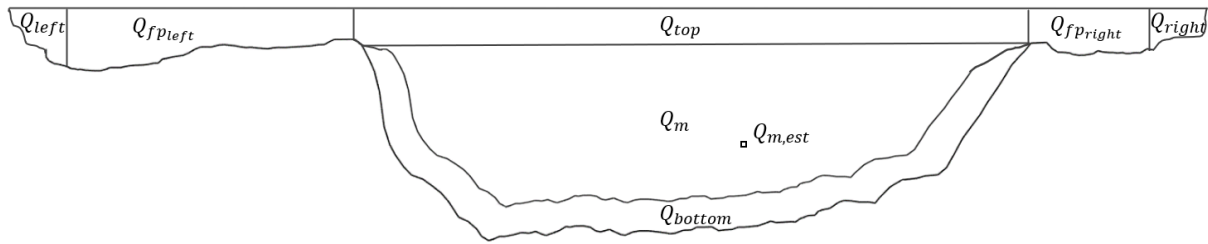


Figure 8: Schematic overview of measured and unmeasured zones in a river cross-section, looking in downstream direction, using the boat-mounted ADCP measuring instrument. Adapted from (J. A. González-Castro & Muste, 2007).

Computed discharge from measurements by the ADCP, Q_m

The total discharge through the measured zones (Q_m) is computed by taking the sum of all discharges through the measured depth-cells (Mueller & Wagner, 2009), see Equation (3). The equation for discharge in a depth-cell is $Q_{bin} = V \cdot A_{bin}$, where V is the average water velocity in the depth-cell and A_{bin} the cross-sectional area of the depth-cell (Mueller & Wagner, 2009).

$$Q_m = \sum_{j=1}^{Ensembles\ Bins} \sum_{i=1}^{Ensembles\ Bins} Q_{bin} = \sum_{j=1}^{Ensembles\ Bins} \sum_{i=1}^{Ensembles\ Bins} |\vec{V}_w| \cdot \sin \theta \cdot W \cdot dz \quad (3)$$

Where,

- Q_{bin} = discharge in a depth-cell [m^3/s]
- $|\vec{V}_w|$ = magnitude of the water velocity vector [m/s]
- θ = internal angle of water velocity vector and boat velocity vector [$^\circ$]
- W = width of ensemble [m]
- dz = depth-cell size [m]
- j = counting index of the ensembles [-]
- i = counting index of the bins [-]

Although AquaVision compared the boat velocity vectors from GPS and bottom-track reference systems to optimise the x - and y -coordinates of the ensembles, they are not provided in the dataset. Therefore, to determine the internal angle θ of the water velocity vector and the boat velocity vector, the tangent vector of the boat's path (i.e., same direction as boat velocity vector) was determined based on the x - and y -coordinates of the ensembles. The width of each ensemble W is determined by the difference in x - and y -coordinates of successive ensembles:

$$W = \sqrt{dy^2 + dx^2} \quad (4)$$

The depth-cell size dz is the vertical difference in z -coordinates of successive depth-cells. This can be set by the ADCP user and is 25 cm for all available measurements.

For a moving-boat ADCP a straight-line transect path is not required to measure the discharge since the magnitude of the water velocity vector is corrected by the internal angle θ to determine the water velocity (TRDI, 2016). To substantiate, Huang (2017) showed in his paper a mathematical proof and field verification that the discharge measured by a moving-boat ADCP is independent from the path of the boat under the assumption that the flow is homogeneous and steady in streamwise direction. This was the case for the ADCP measurements in the main channel.

Estimated discharge for the missing or invalid cells of the measured zone, $Q_{m,est}$

The discharge for the missing or invalid cells in the measured zone is normally estimated by postprocessing interpolation algorithms. In the provided dataset, however, missing or invalid data had already been replaced by Aqua Vision using linear interpolation with neighbouring depth-cells.

Table 3 shows that within the study area only for the Bovenrijn and the Waal, for a limited number of measured transects (i.e., an average of 8% of total number of transects), a few deviating ensembles were removed and replaced by linear interpolation (i.e., an average of 1.2% of total ensembles within these transects). No deviating ensembles were observed in the remaining transects.

Table 3: Overview of ensembles that have been replaced by linear interpolation for the different measurement locations (Eij, 2004).

| Location | Transect | Removed ensembles | Percent of total ensembles [%] |
|-----------|----------|--------------------|--------------------------------|
| Bovenrijn | 4 | 82, 101 | 0.99 |
| | 32 | 36, 78 | 1.02 |
| | 42 | 94 | 0.53 |
| | 48 | 32, 34, 63 | 1.54 |
| | 53 | 28 | 0.50 |
| | 61 | 32, 62, 64, 66, 75 | 2.43 |
| Waal | 6 | 24 | 0.95 |
| | 27 | 49, 61 | 1.94 |
| | 32 | 60 | 1.28 |
| | 50 | 58 | 1.22 |

Estimated discharges for the top and bottom unmeasured zones, Q_{top} and Q_{bottom}

For the discharge in the top and bottom unmeasured zones of the river cross-section, an estimate must be made by extrapolation of the available ADCP water velocities in the measured zone. Choosing the appropriate extrapolation method is based on the software tool Extrap by Mueller (2013), which is also integrated in the U.S. Geological Survey QRev software (Mueller, 2016). Extrap combines normalised velocity profiles of each ensemble in a cross-section and multiple transects to determine one mean velocity profile for all transects in a measurement. Equations (6) and (7) show what the normalised velocity profiles consist of. A single velocity profile is applied to account for natural turbulence and instrument noise in individual ensembles and among transects, under the assumption that hydrodynamic conditions do not change during the measurement with a duration of around 15 minutes. The natural turbulence and instrument noise make it difficult to identify the mean velocity profile for individual ensembles, and Extrap appears to be more accurate and efficient in determining appropriate extrapolation methods compared to standard ADCP manufacturers' software such as WinRiver II and RiverSurveyor (Mueller, 2013). Therefore, the Extrap method is used in choosing the appropriate extrapolation method.

The data must be normalised so that data from shallow parts of the cross-section can be combined with data from deeper parts of the cross-section. The power exponent derived from the normalised data is shown to be valid for use as an exponent in the general power law for estimating the unmeasured top and bottom discharge (Mueller, 2013). This is further explained using the general form of the power law:

$$V_{i,j} = a_j \cdot z_{i,j}^b \quad (5)$$

Where,

| | | |
|-----------|---|---------------------------------|
| $V_{i,j}$ | = | water velocity [m/s] |
| a_j | = | coefficient [1/s] |
| $z_{i,j}$ | = | distance from the streambed [m] |
| b | = | power exponent [-] |

Normalised velocity profiles consist of normalised distances from the streambed ($\hat{z}_{i,j}$) and normalised water velocities ($\hat{V}_{i,j}$). The distance from the streambed is normalised by dividing by the depth from the water surface to the streambed (D_j) for each ensemble:

$$\hat{z}_{i,j} = \frac{z_{i,j}}{D_j} \quad (6)$$

The water velocity is normalised by dividing by the depth-averaged water velocity (\bar{V}_j) in each ensemble:

$$\hat{V}_{i,j} = \frac{V_{i,j}}{\bar{V}_j} \quad (7)$$

The general form of the power law in Equation (5) can be written into the normalised form:

$$\hat{V}_{i,j} = \frac{a_j \cdot D_j^b}{\bar{V}_j} \hat{z}_{i,j}^b = a'_j \cdot \hat{z}_{i,j}^b \quad (8)$$

Where a'_j is a coefficient created from the normalisation process and varying for each ensemble. It can be seen that the power exponent b is the same for both the general and normalised form of the power law.

In this research, the Extrap software method has been reproduced in the MATLAB model since Extrap is not compatible with the ASCII output files generated by Aqua Vision and the required input files (.mmt, .pd0 and r.000) for Extrap were not available in the provided dataset. In addition, a distinction was made between the main channel and the floodplains for determining a mean velocity profile due to the different hydrodynamic conditions in these river sections, which would not have been possible in Extrap. The MATLAB model uses non-linear least squares regression to find an optimised power curve fit and a number of empirically established criteria to choose the most appropriate extrapolation method from the following possible methods (Mueller, 2013):

1. Power fit through the entire profile with a fixed exponent of 0.1667 (default);
2. Power fit through the entire profile with an optimised exponent;
3. Constant fit at the top and a no-slip fit at the bottom with a fixed exponent of 0.1667;
4. Constant fit at the top and a no-slip fit at the bottom 20% of the profile with an optimised exponent;
5. 3-point slope at the top and no-slip fit at the bottom 20% of the profile with a fixed exponent of 0.1667;
6. 3-point slope at the top and no-slip fit at the bottom 20% of the profile with an optimised exponent.

The exponent of 0.1667 is commonly used for fitting the power law to ADCP velocity profiles, since it is more applicable to various flow conditions (J. A. González-Castro & Muste, 2007; Mueller & Wagner, 2009)

The approach will be explained below, a more detailed explanation can be found in the paper by Mueller (2013). Combining and plotting all normalised velocity profiles into one single profile results

in a large cloud of points. To visually assess the appropriateness of the power curve fit, the profile is discretised into 5% increments of normalised distance and for each increment the median and interquartile range of the normalised water velocities and the mean normalised distance from the streambed is calculated. The median normalised water velocity is used instead of the mean to account for possible outliers.

Increments containing less data points than 20% (default value) of the median number of points for all increments are not included in the power curve fitting as these increments could adversely affect the good representation of the velocity profile. A power fit through the 5% increments with a fixed default exponent of 0.1667 is assumed until the data proves that the optimised power fit is better suited. The latter is the case when the coefficient of determination R^2 is greater than or equal to 0.8 and the default exponent is outside the 95% confidence interval of the optimised power exponent.

After that, there are a number of criteria that determine whether the optimised power fit does fit the data well enough or, if not, should be replaced by a constant top and bottom no-slip fit condition. These criteria are partly based on the difference at the water surface between the constant extrapolation and the optimised power fit and the difference at the bottom between the optimised no-slip fit and the optimised power fit. However, this was not the case for the provided data and therefore will not be discussed further. Figure 9 shows the mean velocity profiles for the three branches on 4 November 1998.

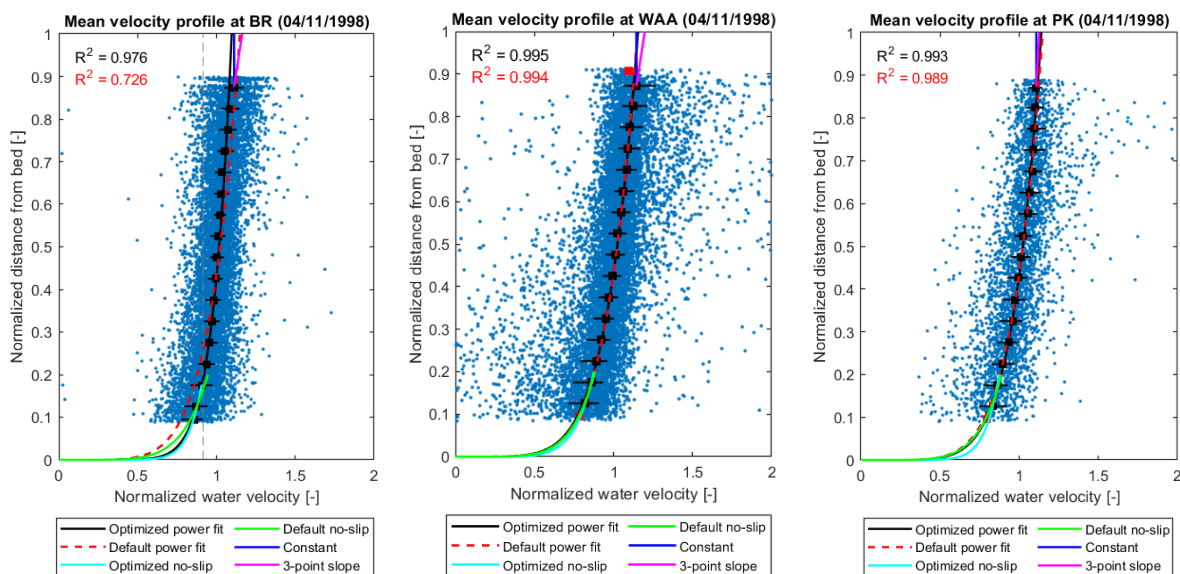


Figure 9: Three plots of normalised data in the main channel showing cloud of points from depth-cells (blue dots), median values for each 5%-increment (black squares), interquartile range for each increment (black whiskers), and the possible extrapolation methods. The R^2 is given for the two power fit extrapolation methods with the default exponent (in red) and the optimised exponent (in black). Left: for the Bovenrijn (BR). Centre: for the Waal (WAA). Right: for the Pannerdensch Kanaal (PK).

For all three river branches, the power curve fit through the entire profile was selected for all measurements, but for the Bovenrijn with an optimised exponent and for the Waal and the Pannerdensch Kanaal with the default exponent. Based on the power curve fit, the unmeasured top discharge was estimated by integrating the power law in Equation (5) over the interval from the top of the topmost depth-cell to the water surface multiplied by the width of each ensemble (J. A. González-Castro & Muste, 2007; Mueller & Wagner, 2009):

$$Q_{top} = \sum_{j=1}^{Ensembles} \frac{a_j}{b+1} (z_{ws}^{b+1} - z_{tb}^{b+1}) \cdot W \quad (9)$$

Where,

- a_j = coefficient derived from a least-squares fit of the equation to the measured data for each ensemble [-]
- b = power exponent [-]
- z_{ws} = distance from the bed to the water surface [m]
- z_{tb} = distance from the bed to the top of the topmost depth-cell [m]
- W = width of ensemble [m]

Where the power exponent b was thus derived from the normalised data for the Bovenrijn or equal to 0.1667 for the Waal and the Pannerdensch Kanaal and fixed for the entire main channel. Using this fixed exponent, coefficient a_j was later determined by least-squares fitting the equation to the original, non-normalised, data in each ensemble (j) of the main channel. The equations for estimating the top discharge using the constant extrapolation method and the 3-point slope fit can be found in Appendix A.

Similar to estimating the top discharge, the discharge in the bottom unmeasured zone of the main channel was estimated by integrating the power law over the interval from the bed to the bottom of the bottom-most depth-cell, assuming the no-slip condition at the bed (Mueller & Wagner, 2009):

$$Q_{bottom} = \sum_{j=1}^{Ensembles} \frac{a_j}{b+1} z_{bb}^{b+1} \cdot W \quad (10)$$

Where,

- z_{bb}^{b+1} = distance from the bed to the bottom of the bottom-most depth-cell [m]

Discharge near the banks, Q_{left} and Q_{right}

The unmeasured discharges at the banks of the river were estimated by interpolation of the water velocity between the riverbank and the nearest ADCP-measured ensemble. The water velocity at the riverbank is equal to zero and the water velocity at the nearest ensemble was measured, to compute the discharge an assumption was made for the bed topography between these points. For the assumption of the bed topography, an edge-shape coefficient was introduced in the following equation for the discharge near the banks (Mueller & Wagner, 2009):

$$Q_{left} = C_{e,left} \cdot V_1 \cdot L_e \cdot h_1, \quad Q_{right} = C_{e,right} \cdot V_m \cdot L_e \cdot h_m \quad (11)$$

Where,

- C_e = edge-shape coefficient [-]
- V = depth-averaged water velocity at nearest ensemble [m/s]
- L_e = distance from the nearest ensemble to the riverbank [m]
- h = water depth at the nearest ADCP-measured ensemble [m]
- Q_{left} = discharge near the left bank [m³/s]
- Q_{right} = discharge near the right bank [m³/s]
- 1 = first ensemble near the left bank [-]
- m = last ensemble near the right bank [-]

The edge-shape coefficient depends on the bed topography near the banks. In cases where the floodplains were inundated, the riverbanks were located near the slope of the dikes and in cases where the water only flowed through the main channel, the riverbanks were located near the slope of the

minor embankments. In both cases there was a triangular shaped bed topography near the banks, so the edge-shape coefficient C_e was set to 0.3535 which assumes a power velocity profile decreasing to zero in the direction of the riverbank (Mueller & Wagner, 2009).

Normally, the ADCP surveyor measures the distances of the unmeasured zones to make a better estimate of the discharge (TRDI, 2016). However, in the dataset provided, the distances from the nearest ensembles to the riverbanks have not been measured. Therefore, Baseline 5.3.3 has been applied to create an elevation model with the dataset *Baseline-Rhine-j95_5-v1*. Although this dataset is from 1995, there were no major human interventions at the ADCP measurement locations in the period from 1995 to 1998. In addition, the Baseline cross-sectional geometries were compared with the AHN1 from 2002 and they show good agreement. Using the elevation model, cross-sectional geometries were generated with the 3D Analyst extension from ArcGIS by importing the x - and y -coordinates of the navigated paths by the moving boat and extending it from dike to dike.

To be able to determine which parts of the cross-section were actually inundated at the time of measuring besides the measured zone of the ADCP, the ADCP cross-sectional geometries were compared with the Baseline cross-sectional geometries. This makes it possible to determine both the distances from the nearest ensembles to the riverbanks and the bed topography more accurately. The data shows that the riverbanks are often situated at the slope of the embankments and therefore the triangular edge-shape coefficient is a good estimate, which can be seen in Figure 10. However, when the unmeasured zone near the edge extends beyond the toe of the dikes, this was counted as floodplain discharge and is further explained in the next section.

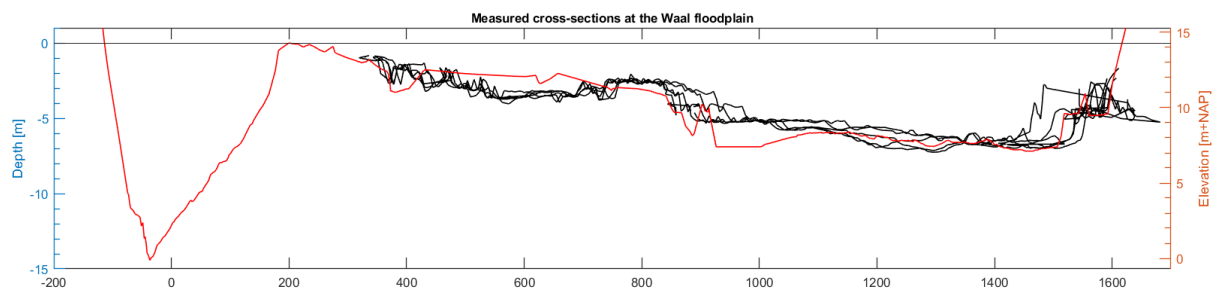


Figure 10: Cross-sectional geometry of the Waal floodplain, the Millingerwaard, based on the measured depths by the ADCP and Baseline.

Estimated discharge through the floodplains, $Q_{fp\text{left}}$ and $Q_{fp\text{right}}$

The discharge through the floodplains is calculated separately from the main channel due to the differences in hydrodynamic conditions. In the period from 3 to 6 November 1998, when ADCP flow measurements were obtained, the floodplains of the Bovenrijn were inundated. The discharge peak occurred on 4 November and then quickly dropped to a discharge where the floodplains were not inundated anymore due to the water level being too low. This was at least the case for the remaining ADCP flow measurements from 9 to 11 November 1998, in the intervening period no ADCP flow measurements were performed.

On the north side of the Waal (at chainage 870.5 km), the main channel is directly bordered by a dike, while on the south side there is a minor embankment that separates the main channel from the Millingerwaard. At the Millingerwaard, ADCP flow measurements were only performed on 4 and 5 November 1998 along a curved navigated path (Figure 11). On these days, the water levels in the main channel did not or hardly exceed the minor embankment, even though these were the highest water levels observed during the measurement campaign. Partly because of this and based on the available ADCP flow measurements, it can be stated that the water in the Millingerwaard was relatively

stagnant. The depth-averaged water velocity vectors are low and point in both up- and downstream direction over the entire navigated path. Negative discharges alternate with positive discharges leading to a low mean discharge.

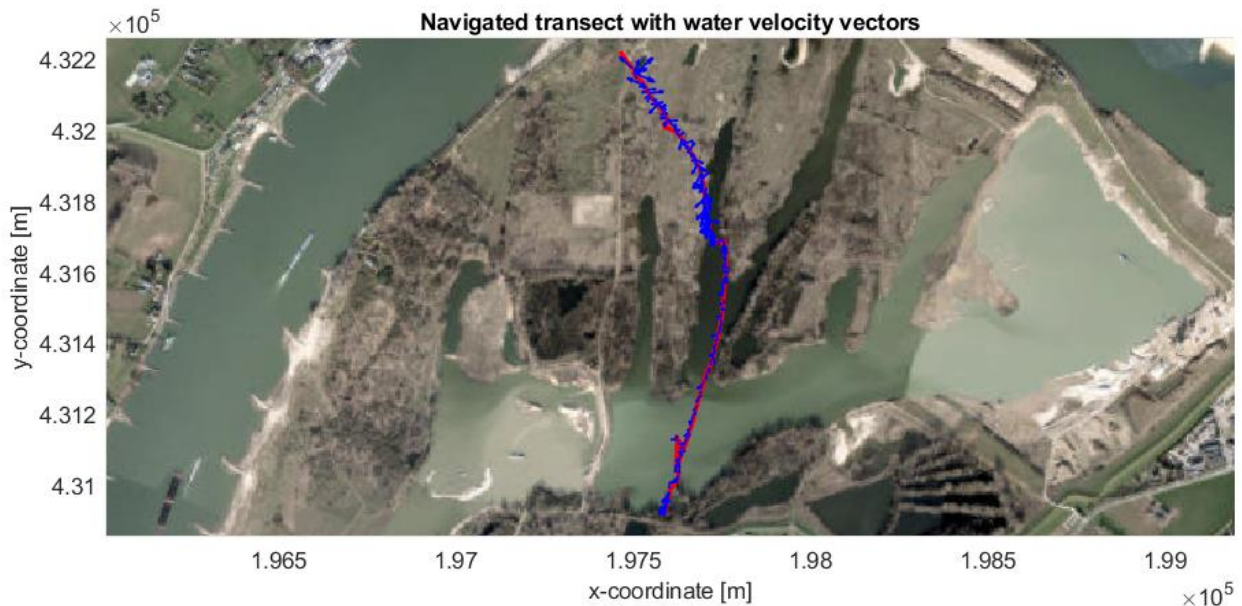


Figure 11: Navigated transect at the Millingerwaard with depth-averaged water velocity vector for an arbitrary measurement.

This can be explained by the fact that in 1998 the Millingerwaard had more of a water storage than a discharge function (Rijkswaterstaat Oost-Nederland, 2000), with result that the water was relatively stagnant during inundation. Later, between 2013 and the present, the Millingerwaard has been redeveloped and a discharge channel was constructed in 2017 and 2018 (Staatsbosbeheer, 2022). In addition, it was regulated that the sequence of flooding in the Millingerwaard first started at the Kekerdomse Waard, which is located downstream of the measurement location (Rijkswaterstaat Oost-Nederland, 2000). This could explain the negative discharges. Furthermore, during the entire period from 3 to 11 November 1998, the Millingse Dam, which regulated the upstream water inflow to the Millingerwaard, was not exceeded by the water level at the Pannerdensche Kop. On 3 and from 6 to 11 November there was no discharge in the Millingerwaard.

In the period from 4 to 6 November 1998, when ADCP flow measurements were obtained, the floodplains of the Pannerdensch Kanaal were inundated. On 9 and 10 November no more flow measurements could be performed due to the water level being too low and after that (e.g., on 11 November) the floodplains were no longer inundated. To the right of the minor embankment there is a small lake called the Zorgdijkplas, which connected to a weir (i.e., the Pannerdensche Overlaat) that regulated the water inflow to the green river along the Pannerdensch Kanaal at high discharges (Visser & Klopstra, 2002). These discharges were obtained for the period 3 to 11 November 1998 using a rating curve developed by the Waterloopkundig Laboratorium, which was not maintained at the time (Visser & Klopstra, 2002). The water levels were measured by a float-driven shaft encoder. The uncertainty of this rating curve is estimated based on the handbook by Hartong & Termes (2009) and is 5% of the estimated discharge for a measuring weir.

When ADCP flow measurements are available in the floodplains, estimating the discharge through the top and bottom unmeasured zones of the floodplains is performed according to the same principle as estimating the top and bottom discharge of the main channel. The only difference is that the no-slip condition for the power fit is not applied at the bed since the floodplains are covered with different

types of vegetation. Therefore, a hydraulic roughness parameter describing the characteristic hydraulic friction length (z_0) is introduced into the power law:

$$V_{i,j} = a_j \cdot (z_{i,j} - z_0)^b \quad (12)$$

Where,

| | | |
|-----------|---|---|
| $V_{i,j}$ | = | water velocity [m/s] |
| a_j | = | coefficient [1/s] |
| $z_{i,j}$ | = | distance from the streambed [m] |
| z_0 | = | height above the streambed where the velocity is zero [m] |
| b | = | power exponent [-] |

A general expression for z_0 for shallow-water flows and hydraulic rough walls is as follows (Vermeulen et al., 2019):

$$z_0 = \frac{k_N}{33} \quad (13)$$

Where,

| | | |
|-------|---|--------------------------------|
| k_N | = | Nikuradse roughness height [m] |
|-------|---|--------------------------------|

The floodplains at the measurement locations in the Bovenrijn, the Pannerdensch Kanaal, the Nederrijn and the IJssel all consist of grassland which, according to the Handbook flow resistance vegetation in floodplains, has a Nikuradse roughness height of 0.1 m (Van Velzen et al., 2003). The floodplain at the the Waal, the Millingerwaard, consists of grass, shrubbery and trees. However, at the navigated boat path, there is a trench with standing water surrounded by grass which has a Nikuradse roughness height of 0.15 m (Van Velzen et al., 2003).

z_0 is normalised by dividing by the depth from the water surface to the streambed (D_j), which results in the following normalised form of the power law:

$$\hat{V}_{i,j} = a'_j \cdot (\hat{z}_{i,j} - \hat{z}_0)^b \quad (14)$$

This power law has been used in the non-linear least squares regression to find an optimised power curve fit to the mean velocity profile in the floodplains and the mean velocity profiles for the three branches are shown in Figure 19 of Appendix B.

The floodplain discharge consists of the computed discharge in the measured zone and estimated discharges in the top and bottom unmeasured zones based on the selected extrapolation method.

Only for the Pannerdensch Kanaal no ADCP flow measurements were performed on 9 and 10 November 1998, while the floodplains were inundated with a low water level. For the other river branches ADCP flow measurements were always performed when the floodplains were inundated. In this case, the discharge was estimated based on Equation (11) for the edge discharge, where the edge-shape coefficient (C_e), the water depth at the nearest ADCP-measured ensemble (h) and the edge distance (L_e) were substituted for the Baseline bed topography to make a more accurate estimate of the cross-sectional area of the floodplains. The depth-average water velocity at the nearest ensemble has been applied and a power velocity profile decreasing to zero in the direction of the riverbank has also been adopted to account for decreasing water velocities above the floodplains. The uncertainty of this estimate of the floodplain discharge is approached the same as the edge discharge uncertainty.

3.3.2 Possible uncertainties in the measuring procedure and weight of each uncertainty

Because of assumptions and estimates made in the procedure to determine the total discharge, possible errors arise between the computed total discharge and the actual total discharge. These possible errors lead to uncertainties in the computed discharge. In an effort to quantify these uncertainties, the following uncertainty propagation methods for moving-boat ADCP measurements have been recently developed: OURSIN (Pierrefeu et al., 2017), QUant (Moore et al., 2017), RiverFlowUA (J. González-Castro et al., 2016) and QRev (Mueller, 2016). These propagation methods are based on the Guide to the Expression of Uncertainty in Measurement (JCGM, 2008), which provides internationally standardised rules for evaluating and expressing uncertainty in measurements. The uncertainty analysis in this research is based on the QRev software (Mueller, 2016), which is a simplistic approach that combines the uncertainty due to random errors, invalid data, estimated edge discharges, extrapolated top and bottom discharges, moving bed and systematic errors. Although the approach is simplistic, QRev is the only method from the mentioned uncertainty propagation methods that is part of routine procedures in U.S. Geological Survey and other hydrometric agencies around the world (Hauet, 2020).

The uncertainty due to invalid data is negligible, since on average only 0.15% of the invalid data has been replaced for the Bovenrijn and the Waal (Eij, 2004). For the other measurement locations, no invalid data were observed at all. Furthermore, the uncertainty due to moving bed is also not included since Aqua Vision has corrected for the occurrence of a moving bed by replacing the bottom-track navigational reference with GPS navigational reference. Therefore, these uncertainty sources are not included in the uncertainty analysis, which is now divided into the following categories:

Random uncertainty, u_{random}

The random error in a moving-boat ADCP measurement is typically estimated by the coefficient of variation of the total discharge for all transects, which is a measure of variability in relation to the mean total discharge of all transects (Moore et al., 2017). The coefficient of variation for the total discharge Q_{tot} was calculated by dividing the standard deviation (σ) of the total discharge from all transects by the mean discharge (\bar{Q}_{tot}) of these transects.

$$Q_{Cov} (\%) = \frac{\sigma_{Q_{tot}}}{\bar{Q}_{tot}} \cdot 100\% \quad (15)$$

The random uncertainty with a 95% confidence interval was calculated by multiplying the coefficient of variation (Q_{Cov}) with the coverage factor from the Student's t -distribution with $M-1$ degrees of freedom divided by the square root of the number of transects (M) within one measurement.

$$u_{random} = Q_{Cov} \cdot \frac{t}{\sqrt{M}} \quad (16)$$

The Student's t -value was obtained using the MATLAB function `tinvs` for a two-tailed 95% confidence interval and $M-1$ degrees of freedom.

Edge discharge uncertainty, u_{edge}

The edge discharge uncertainty with a 95% confidence interval in QRev is assumed to be 30% of the total edge discharge. However, to account for the uncertainty of the individual variables in the edge discharge computation (Equation (11)), estimates by Moore et al. (2017) were adopted in this research instead of the standard QRev assumption. Moore et al. (2017) estimated the uncertainty of the edge-shape coefficient to be $\pm 10\%$ of its original value and the uncertainty of the edge distance to be $\pm 30\%$ of its original value, based on field experience. Furthermore, the uncertainty of the depth-averaged water velocity at the nearest ensemble is defined as the standard deviation of all water velocities in

the nearest ensemble (Moore et al., 2017). In particular, the standard deviation of the water velocity has a major influence on the uncertainty in the edge discharge.

Extrapolation uncertainty, $u_{extrapolation}$

Discharge measurement errors are partly due to inaccurate estimation of discharge through the unmeasured zones. Therefore, the extrapolation uncertainty is determined by computing the percent difference in the total discharge from the selected extrapolation method to other possible extrapolation methods and averaging of the four best methods for the floodplains, top and bottom unmeasured zones.

ADCP velocity uncertainty, $u_{velocity}$

To determine the uncertainty due to the velocity accuracy of the ADCP instrument, a sensitivity analysis was performed in which the velocity magnitude was varied by plus minus the velocity accuracy to outline its influence on the computed total discharge. The velocity accuracy for the RD Instruments ADCP 1200 kHz BroadBand is ± 2.5 mm/s the water velocity relative to the ADCP instrument (TRDI, 2007).

Bottom depth uncertainty, u_{depth}

For the bottom depth, the ADCP is assumed to meet the manufacturer's specifications, which has an accuracy of ± 1 cm (TRDI, 2007). Similar to the ADCP velocity accuracy, the bottom depth is varied in a sensitivity analysis by ± 1 cm.

Systematic uncertainty, $u_{systematic}$

The systematic uncertainty is caused by systematic errors, which are almost impossible to quantify because it requires knowledge of the correlation between error sources as well as experimental measurements (J. A. González-Castro & Muste, 2007). Due to lack of data an estimate was made based on QRev and Huang (2018b). The systematic uncertainty is assumed to be constant for each measurement with 1.5% at one standard deviation of the total discharge from all transects (Mueller, 2016), which can be expanded to a 95% confidence interval by multiplying it with the coverage factor (k_p) of 1.96 (JCGM, 2008). This yields an expanded uncertainty of 2.94% of the total discharge. 1.5% is in line with the systematic uncertainty for moving-boat ADCP discharge measurements of 1.55% estimated by Huang (2018b), which has accounted for almost all systematic errors encountered in a large number of validated ADCP comparison datasets based on classical error analysis techniques.

Overall uncertainty, $u_{Q_{tot}}$

The overall uncertainty (i.e., uncertainty of total discharge, $u_{Q_{tot}}$) with a 95% confidence interval is estimated by taking the root-sum-of-squares of the individual uncertainty sources (at 95% confidence level) in Equation (17), assuming each uncertainty source is uncorrelated. This standard approach is based on the Guide to the Expression of Uncertainty in Measurement (JCGM, 2008). The final estimated uncertainty should not be viewed as strictly quantitative but more as a best-guess estimate since the quantifying the various sources of uncertainty is based on approximations and assumptions.

$$u_{Q_{tot}} = \sqrt{u_{random}^2 + u_{edge}^2 + u_{extrapolation}^2 + u_{velocity}^2 + u_{depth}^2 + u_{systematic}^2} \quad (17)$$

Where,

| | | |
|---------------------|---|--|
| u_{random} | = | random uncertainty [m ³ /s] |
| u_{edge} | = | edge discharge uncertainty [m ³ /s] |
| $u_{extrapolation}$ | = | extrapolation uncertainty [m ³ /s] |
| $u_{velocity}$ | = | ADCP velocity uncertainty [m ³ /s] |
| u_{depth} | = | bottom depth uncertainty [m ³ /s] |
| $u_{systematic}$ | = | systematic uncertainty at 95% confidence level [m ³ /s] |

Furthermore, the uncertainty has also been estimated for all discharge components in Equation (2) individually to gain more insight into the contribution of the uncertainty of each discharge component to the uncertainty of the total discharge. This results in the uncertainty of the left edge discharge ($u_{Q_{left}}$), the left floodplain discharge ($u_{fp_{left}}$), the top discharge ($u_{Q_{top}}$), the measured discharge (u_{Q_m}), the bottom discharge ($u_{Q_{bottom}}$), the right floodplain discharge ($u_{fp_{right}}$) and the right edge discharge ($u_{Q_{right}}$). Prior to that, the uncertainty due to random errors, extrapolation, velocity accuracy, bottom depth accuracy and systematic errors has been determined for all discharge components individually.

The root-sum-of-squares could also be applied to the individual uncertainties of all discharge components to determine uncertainty of the total discharge. However, the problem with the root-sum-of-squares is that it is only valid under the assumption that each discharge component is uncorrelated. However, a correlation analysis of the discharge components has been performed and shows that the discharge components are correlated. As a result, the overall uncertainty based on the root-sum-of-squares of the uncertainties of all discharge components underestimated the outcome of Equation (17) since correlations between the discharge components are not included. Therefore, the standard approach in Equation (17) is applied to determine the overall uncertainty.

3.4 The uncertainty of the total discharges in the branches and the water balance of the Pannerdensche Kop

Operational rating curves during the period of November 1998 were located up- and downstream in the branches of the Pannerdensche Kop (Figure 12). A near perfect water balance would be expected between those rating curves as there is no other major branch where water is entering or leaving the system. Twijnstra et al. (2020), however, showed in his research that there is a water balance error between the branches at the Pannerdensche Kop.

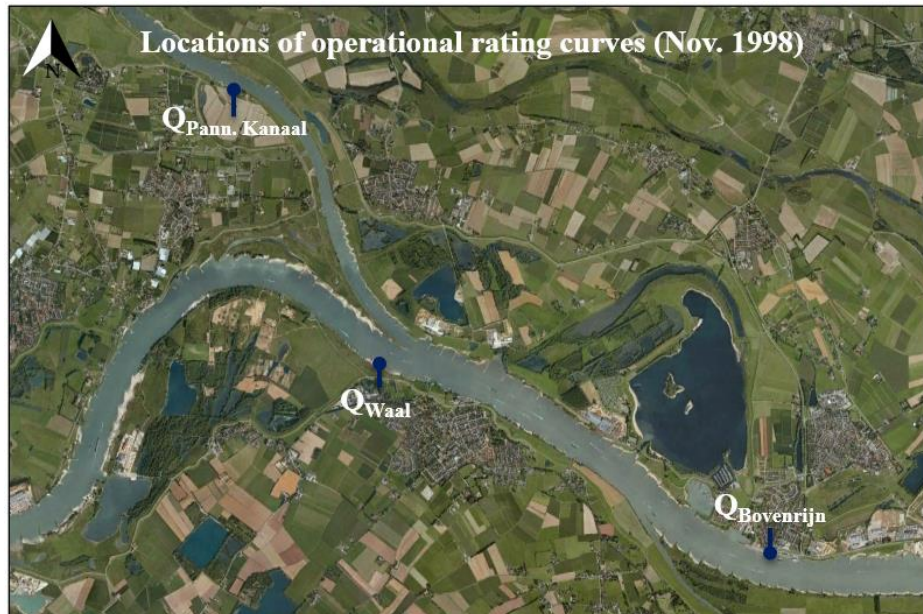


Figure 12: Locations of the operational rating curves in the branches of the Pannerdensche Kop during the period 3-11 November 1998 (retrieved from <https://waterinfo.rws.nl/>).

To determine which rating curve is the most uncertain in terms of uncertainty of the estimated discharge values, the differences in the degree of uncertainty were outlined by reconstructing the total discharge with the available ADCP measurements and performing an uncertainty analysis for the Bovenrijn, the Waal and the Pannerdensch Kanaal. Subsequently, the estimated ADCP discharges with 95% uncertainty bandwidths were compared with the historical derived discharges during the period 3 to 11 November 1998 from the nearest measuring stations. The nearest stations with available measurements for the Bovenrijn (Rkm 863.9), the Waal (Rkm 870.5) and the Pannerdensch Kanaal (Rkm 869.0) are located at Lobith (Rkm 863.0), the Pannerdensche Kop (Rkm 867.5) and Pannderden (Rkm 872.0) respectively (Figure 12). The distance to the station is smallest for the Bovenrijn, 900 m upstream, the Waal and the Pannerdensch Kanaal both have the same distance to the stations (i.e., 3 km up- and downstream respectively).

The discharge data derived from the operational rating curves has a 10-minute interval and are publicly available via (<https://waterinfo.rws.nl/>). Table 4 shows which discharge stations were used for the up- and downstream branches at the Pannerdensche Kop.

Table 4: Location of nearest discharge station with available continuous discharge measurements.

| Branch | Discharge station | Chainage [km] |
|--------------------------|-------------------|---------------|
| Bovenrijn (BR) | Lobith | 863.0 |
| Waal (WAA) | Pannerdensche Kop | 867.5 |
| Pannerdensch Kanaal (PK) | Pannderden | 872.0 |

In 1998, the rating curves were adjusted if the periodically measured discharges differ by more than 5% from the discharges obtained from the operational rating curves. The rating curves were adjusted once every 4 to 5 years and the last adjustments date from 1996 (Visser & Klopstra, 2002). At a water level higher than 14 m+NAP at Lobith, discharge measurements in the Bovenrijn were performed at the chainage 863.9 km.

The Water Balance Error (WBE) at the Pannerdensche Kop was determined for the measured ADCP discharges as for the available historical same-day derived discharges. The Water Balance Error (WBE) was determined by the following equation based on (Gensen, 2021):

$$WBE = (Q_{BR} - Q_{WAA} - Q_{PK})/Q_{BR} \cdot 100\% \quad (18)$$

Where,

- Q_{BR} = upstream discharge at the Pannerdensche Kop in the Bovenrijn (BR) [m³/s]
- Q_{WAA} = downstream discharge at the Pannerdensche Kop in the Waal (WAA) [m³/s]
- Q_{PK} = downstream discharge at the Pannerdensche Kop in the Pannerdensch Kanaal (PK) [m³/s]

Both the measured discharges by the ADCP and the historical derived discharges were not all obtained directly at the Pannerdensche Kop, but further up- and downstream. To make use of the physical constraint of water balance closure at the Pannerdensche Kop, the discharges were daily averaged under the assumption that this eliminated possible water balance errors due to the time delay between the different locations (Gensen, 2021). It was analysed whether uncertainties in the discharges of the three branches can explain the water balance error at the Pannerdensche Kop. For that, the propagation of the uncertainties in the discharges of each branch to the uncertainty in the water balance error at a 95% confidence interval was determined by the following equation, based on the Guide to the Expression of Uncertainty in Measurement (JCGM, 2008):

$$u_{WBE} = WBE \sqrt{\frac{u_{BR}^2 + u_{WAA}^2 + u_{PK}^2}{(Q_{BR} - Q_{WAA} - Q_{PK})^2} + \left(\frac{u_{BR}}{Q_{BR}}\right)^2} \cdot 100\% \quad (19)$$

Where,

- u_{BR} = uncertainty of total discharge in the Bovenrijn [m³/s]
- u_{WAA} = uncertainty of total discharge in the Waal [m³/s]
- u_{PK} = uncertainty of total discharge in the Pannerdensch Kanaal [m³/s]

4 Results

4.1 Uncertainties in high river discharge measurements and their weight on the overall uncertainty

All discharge components leading to the total discharge were computed and estimated for the three river branches around the Pannerdensche Kop; the Bovenrijn (BR), the Waal (WAA) and the Pannerdensche Kanaal (PK); and are listed in Table 5.

Table 5: Overview of all calculated and estimated discharge components for the three river branches around the Pannerdensche Kop.

| Location | Date | Time | Tr. | Q_{left} | $Q_{fp_{left}}$ | Q_{top} | Q_m | Q_{bottom} | $Q_{fp_{right}}$ | Q_{right} | Q_{tot} |
|----------|--------|-------|------|---------------------|---------------------|---------------------|---------------------|---------------------|---------------------|---------------------|---------------------|
| | | | [#] | [m ³ /s] |
| BR | 3-Nov | 13:11 | 4 | 11.4 | 351.0 | 1189.9 | 7088.8 | 672.9 | 38.3 | 6.5 | 9358.9 |
| | 4-Nov | 13:18 | 3 | 12.6 | 467.4 | 1183.6 | 7282.6 | 717.4 | 59.6 | 5.4 | 9728.6 |
| | 4-Nov | 16:27 | 5 | 13.9 | 454.4 | 1176.5 | 7184.8 | 671.6 | 56.5 | 6.5 | 9564.3 |
| | 5-Nov | 12:26 | 3 | 6.8 | 435.7 | 1138.2 | 6839.7 | 650.2 | 43.0 | 10.1 | 9123.7 |
| | 5-Nov | 16:36 | 3 | 9.9 | 430.8 | 1176.2 | 6841.3 | 642.6 | 61.2 | 6.3 | 9168.3 |
| | 6-Nov | 11:34 | 5 | 12.5 | 315.9 | 1055.0 | 6251.5 | 594.2 | 22.1 | 3.2 | 8254.5 |
| | 6-Nov | 15:48 | 4 | 8.2 | 312.1 | 1028.3 | 6162.4 | 596.2 | 15.2 | 1.4 | 8123.8 |
| | 9-Nov | 12:21 | 5 | 14.4 | 0.4 | 882.5 | 4728.4 | 480.8 | 0.0 | 11.9 | 6118.3 |
| | 9-Nov | 16:30 | 5 | 15.3 | 1.0 | 864.2 | 4563.1 | 481.0 | 0.5 | 12.5 | 5937.8 |
| | 10-Nov | 11:55 | 5 | 15.3 | 0.4 | 834.5 | 4318.3 | 442.7 | -0.2 | 5.8 | 5616.7 |
| | 10-Nov | 16:01 | 5 | 17.0 | 0.7 | 843.8 | 4324.0 | 450.6 | -0.1 | 6.6 | 5642.7 |
| 11-Nov | 13:47 | 5 | 8.8 | 0.7 | 805.9 | 4035.9 | 422.5 | 0.4 | 4.4 | 5278.5 | |
| 11-Nov | 17:08 | 5 | 19.1 | 0.8 | 806.8 | 4073.0 | 442.8 | 0.1 | 4.7 | 5347.2 | |
| WAA | 3-Nov | 16:35 | 5 | 15.1 | 1.4 | 923.4 | 4803.1 | 458.9 | 0.4 | 15.5 | 6217.8 |
| | 4-Nov | 11:24 | 4 | 19.8 | 7.4 | 944.1 | 4916.2 | 450.8 | 0.7 | 13.1 | 6352.0 |
| | 4-Nov | 14:40 | 3 | 37.1 | 8.9 | 891.3 | 4731.6 | 465.9 | 0.1 | 9.1 | 6144.0 |
| | 5-Nov | 10:35 | 5 | 24.7 | 8.8 | 878.9 | 4615.0 | 471.4 | 0.6 | 10.9 | 6010.3 |
| | 5-Nov | 14:24 | 3 | 13.6 | 9.5 | 911.0 | 4649.5 | 425.5 | 0.6 | 10.3 | 6020.0 |
| | 6-Nov | 09:47 | 4 | 18.5 | 0.3 | 858.9 | 4358.5 | 441.3 | 0.6 | 25.7 | 5703.7 |
| | 6-Nov | 14:06 | 3 | 29.5 | 0.8 | 839.5 | 4131.5 | 392.4 | 0.7 | 11.7 | 5406.0 |
| | 9-Nov | 09:53 | 3 | 17.1 | -0.2 | 680.6 | 3016.0 | 316.3 | 3.6 | 8.3 | 4041.6 |
| | 10-Nov | 09:54 | 5 | 9.3 | 0.4 | 687.3 | 2960.0 | 329.5 | 3.5 | 4.7 | 3994.6 |
| | 10-Nov | 14:12 | 5 | 4.2 | 0.1 | 670.8 | 2921.9 | 331.8 | 1.6 | 4.0 | 3934.3 |
| | 11-Nov | 12:06 | 5 | 5.0 | -0.1 | 655.4 | 2724.7 | 324.8 | 3.5 | 8.5 | 3721.7 |
| 11-Nov | 15:26 | 5 | 15.9 | 0.2 | 655.1 | 2661.2 | 310.0 | 1.8 | 8.0 | 3652.3 | |
| PK | 3-Nov | 09:14 | 3 | 3.1 | 41.3 | 476.3 | 2173.9 | 222.5 | 274.6 | 18.1 | 3209.7 |
| | 4-Nov | 14:04 | 3 | 3.9 | 50.9 | 489.9 | 2155.3 | 231.8 | 292.8 | 15.1 | 3239.6 |
| | 4-Nov | 09:45 | 3 | 0.9 | 49.1 | 485.6 | 2152.7 | 213.4 | 247.8 | 13.5 | 3163.0 |
| | 5-Nov | 13:49 | 4 | 2.7 | 31.6 | 477.9 | 2115.5 | 221.4 | 235.5 | 16.4 | 3100.9 |
| | 5-Nov | 09:15 | 3 | 1.4 | 33.6 | 430.4 | 1858.2 | 193.7 | 114.4 | 14.3 | 2645.9 |
| | 6-Nov | 13:23 | 3 | 1.0 | 50.5 | 447.8 | 1958.9 | 217.3 | 81.8 | 16.9 | 2774.2 |
| | 6-Nov | 09:23 | 4 | 27.1 | 2.4 | 331.7 | 1423.1 | 149.8 | 0.2 | 30.0 | 1964.4 |
| | 9-Nov | 13:10 | 5 | 39.0 | 2.3 | 336.9 | 1386.2 | 151.3 | 0.2 | 19.8 | 1935.6 |
| | 9-Nov | 09:11 | 5 | 19.6 | 4.0 | 316.9 | 1333.6 | 147.0 | 2.3 | 33.2 | 1856.6 |
| | 10-Nov | 13:34 | 5 | 41.2 | 1.8 | 300.0 | 1261.5 | 145.6 | 2.3 | 22.3 | 1774.6 |
| | 10-Nov | 09:25 | 5 | 30.5 | 1.8 | 296.6 | 1216.5 | 127.5 | 1.8 | 24.7 | 1699.4 |
| 11-Nov | 11:30 | 5 | 60.3 | 0.1 | 292.0 | 1196.2 | 130.1 | 1.7 | 25.8 | 1706.1 | |
| 11-Nov | 14:42 | 5 | 33.8 | 1.4 | 309.1 | 1274.6 | 139.3 | 0.7 | 24.4 | 1783.2 | |

Note. The discharges are averaged over multiple transects (Tr.) per measurement. A row represents a measurement performed on different dates and times. The time is listed as the time halfway through the ADCP flow measurement.

Table 5 shows that the highest total discharge occurred on 4 November for all branches, after that the total discharge decreased with time. This pattern is observed for all discharge components, except for some edge discharges and this is mainly because the measuring boats were able to measure closer to the riverbanks during higher water levels. In that case, a higher discharge was included in the measured portion of the adjacent floodplain.

In Figure 13, all individual discharge components are plotted in a bar graph for each measurement and river branch. The measured discharge in the main channel is by far the largest, and fairly constant, contributor to the total discharge. The contribution of the measured discharge to the total discharge is relatively large with an average of 75.9%, 75.6% and 70.1% for the Bovenrijn, the Waal, the Pannerdensch Kanaal respectively (see Table 6). The lowest percentage for the Pannerdensch Kanaal is due to relatively higher ratio of the top unmeasured zone to the measured zone, and thus of the unmeasured top discharge to the total discharge, compared to the Bovenrijn and the Waal. The Pannerdensch Kanaal also had a higher ratio of the unmeasured floodplain and edge discharges to the total discharge, mainly due to the discharge in the Zorgdijkplas.

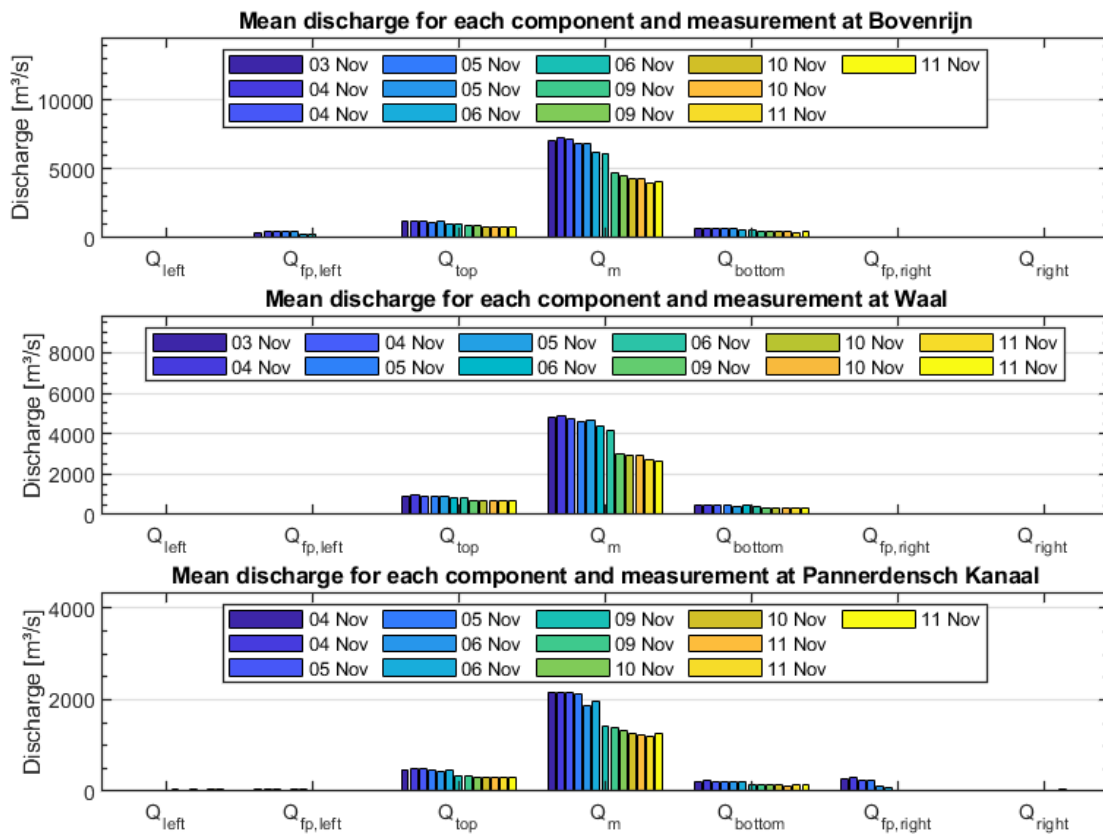


Figure 13: Bar plot of the mean discharge for each component and measurement at all three measuring locations around the Pannerdensch Kop.

After the measured discharge, the top and bottom discharge make the second and third largest contribution to the total discharge.

Table 6: Average contribution of discharge components to the total discharge in percentage over all measurements for each location.

| Location | Q_{left} [%] | $Q_{fp_{left}}$ [%] | Q_{top} [%] | Q_m [%] | Q_{bottom} [%] | $Q_{fp_{right}}$ [%] | Q_{right} [%] | Q_{tot} [%] |
|----------|-------------------|------------------------|------------------|--------------|---------------------|-------------------------|--------------------|------------------|
| BR | 0.19 | 2.35 | 13.62 | 75.94 | 7.57 | 0.25 | 0.09 | 100 |
| WAA | 0.33 | 0.05 | 15.93 | 75.63 | 7.81 | 0.04 | 0.21 | 100 |
| PK | 1.11 | 0.71 | 16.41 | 70.12 | 7.51 | 3.14 | 1.00 | 100 |

4.1.1 Uncertainties in the measuring procedure and the weight of each uncertainty

Individual uncertainty sources

The individual uncertainty sources consist of the random uncertainty, edge uncertainty, extrapolation uncertainty, systematic uncertainty, velocity accuracy uncertainty and bottom depth uncertainty (see Section 3.3.2). The uncertainty sources (at a 95% confidence level) are plotted in absolute values (in m^3/s) of the total discharge for each measurement and for all river branches (see Figure 14). The y-axes have equal scales to allow for better comparison between the branches.

The random uncertainty and systematic uncertainty have the most influence on the expanded uncertainty of the total discharge. The systematic uncertainty is assumed constant for each measurement with a 95% confidence level of 2.94%, while the random uncertainty depends on the coefficient of variation of the total discharge (Q_{COV}) for all transects and the number of transects. The coefficient of variation represents the natural turbulence and instrument noise between the successive transects, assuming that the ADCP user has performed self-consistent measurements.

The uncertainties in the Bovenrijn are fairly constant over all measurements based on Figure 14 and this observation is even more supported by the uncertainties relative to the total discharge (Figure 20). This is because larger absolute uncertainties are compensated for by larger total discharges and vice versa.

At the Waal, there is more fluctuation in the uncertainties over all measurements. High uncertainties are due to high random uncertainties and the opposite applies to low uncertainties. This phenomenon is mainly caused by the coefficients of variation of the total discharges and there appears to be a negative correlation with the number of navigated transects (see Table 7 and Figure 21). Measurements with the highest uncertainties have the least number of transects (i.e., 3) and the lowest uncertainties have the most transects (i.e., 5). It is known that a higher number of successive transects is important for reducing the uncertainty in ADCP measurements, where a minimum of four transects is recommended (Oberg & Mueller, 2007).

The Pannerdensch Kanaal has the smallest uncertainties in absolute terms of the three river branches, but also the smallest total discharge, so that the relative uncertainties are larger than the Bovenrijn and comparable to the Waal. A causality between the uncertainties and the coefficients of variation is found and, in contrast to the Waal, there appears to be no correlation with the number of transects (Table 7 and Figure 21).

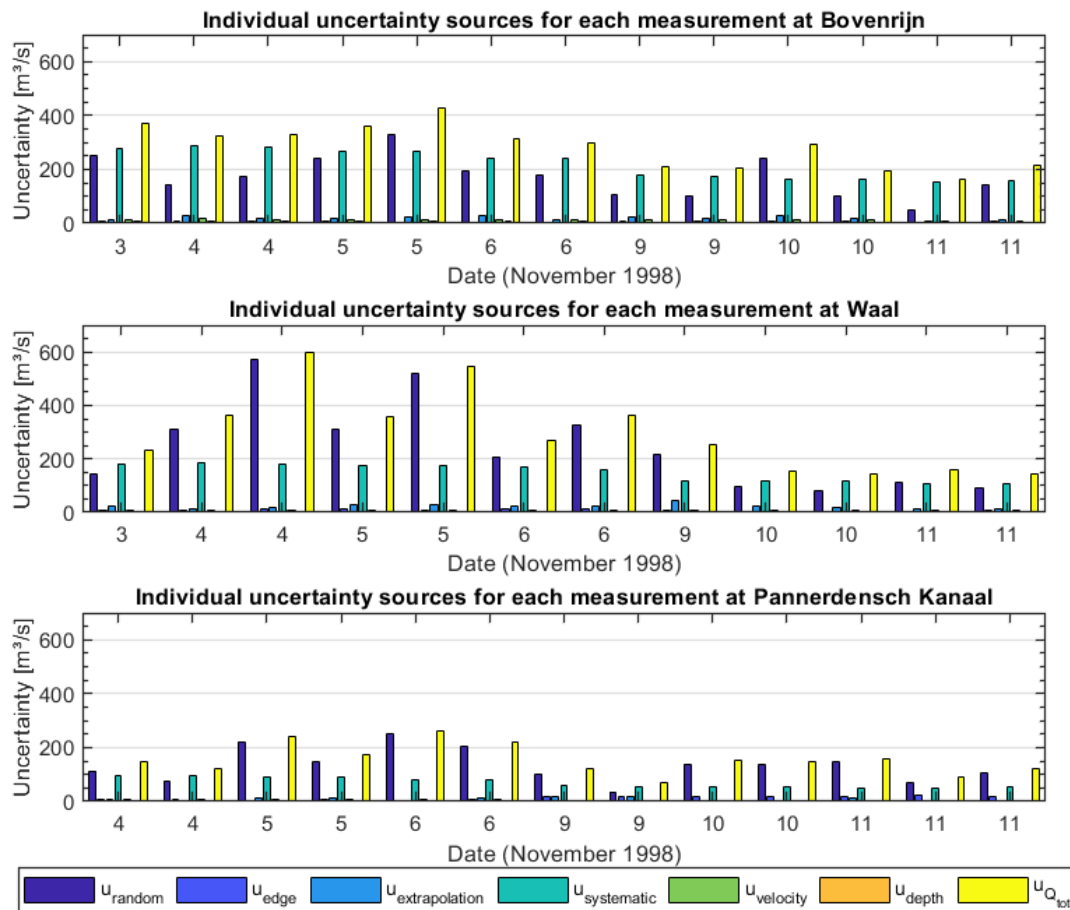


Figure 14: Individual uncertainty sources (at 95% confidence level) over time for the three river branches, with absolute values in m³/s.

The uncertainty of the estimated edge discharge, ADCP velocity accuracy and bottom depth accuracy proves to be negligible under the current circumstances. This is explained by the small fraction of the edge discharge relative to the total discharge and the relatively high accuracy of the ADCP instrument, also because of the relatively high flow velocities. Oberg & Mueller (2007) showed that an ADCP instrument is more accurate at higher flow velocities.

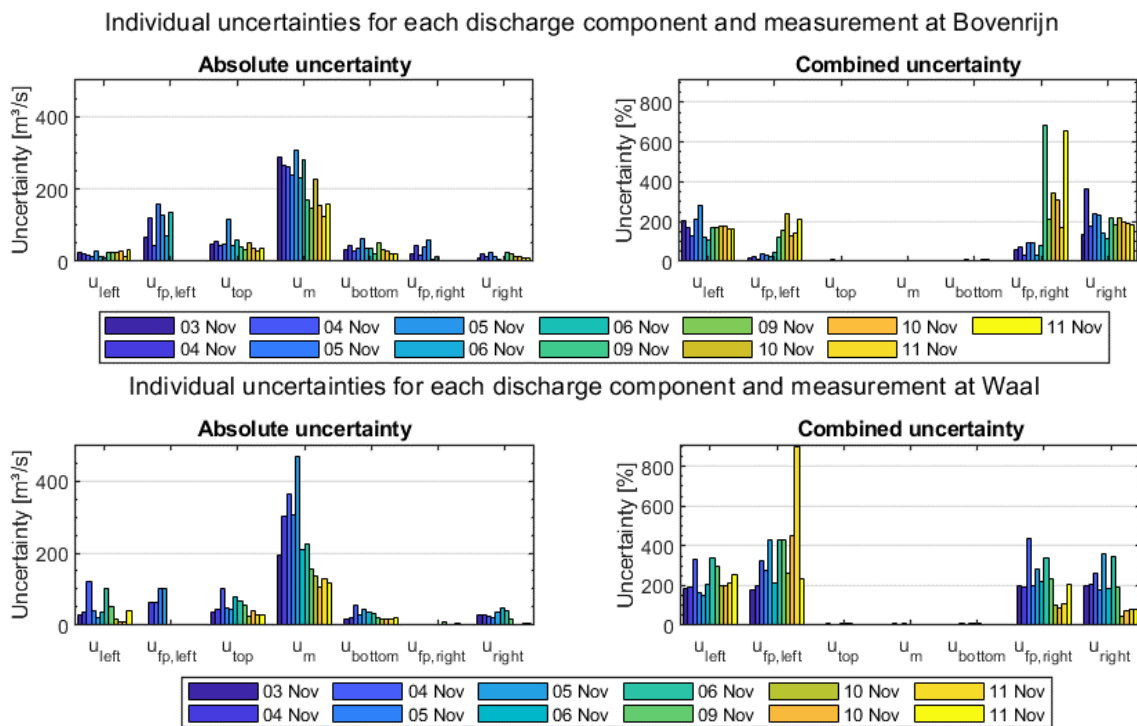
Table 7: A complete overview of the number of transects, the coefficient of variation, the mean total discharge and the uncertainty of the total discharge in cubic meters per second and percentage for each measurement location.

| | | | | | | | | | | | | | | |
|---|------------|--------|--------|--------|--------|--------|--------|--------|--------|--------|--------|--------|--------|--------|
| Date | 3-Nov | 4-Nov | 4-Nov | 5-Nov | 5-Nov | 6-Nov | 6-Nov | 9-Nov | 9-Nov | 10-Nov | 10-Nov | 11-Nov | 11-Nov | 11-Nov |
| Location | <u>BR</u> | | | | | | | | | | | | | |
| Time | 13:11 | 13:18 | 16:27 | 12:26 | 16:36 | 11:34 | 15:48 | 12:21 | 16:30 | 11:55 | 16:01 | - | 13:47 | 17:08 |
| Transects [#] | 4 | 3 | 5 | 3 | 3 | 5 | 4 | 5 | 5 | 5 | 5 | - | 5 | 5 |
| Q_{CoV} [%] | 1.67 | 0.60 | 1.45 | 1.05 | 1.45 | 1.90 | 1.37 | 1.39 | 1.40 | 3.47 | 1.46 | - | 0.73 | 2.14 |
| Q_{tot} [m³/s] | 9358.9 | 9728.6 | 9564.3 | 9123.7 | 9168.3 | 8254.5 | 8123.8 | 6118.3 | 5937.8 | 5616.7 | 5642.7 | - | 5278.5 | 5347.2 |
| $u_{Q_{tot}}$ [m³/s] | 371.5 | 322.0 | 330.9 | 359.5 | 426.3 | 312.8 | 298.1 | 210.5 | 204.3 | 294.9 | 196.4 | - | 163.1 | 212.8 |
| $u_{Q_{tot}}$ [%] | 3.97 | 3.31 | 3.46 | 3.94 | 4.65 | 3.79 | 3.67 | 3.44 | 3.44 | 5.25 | 3.48 | - | 3.09 | 3.98 |
| Location | <u>WAA</u> | | | | | | | | | | | | | |
| Time | 16:35 | 11:24 | 14:40 | 10:35 | 14:24 | 09:47 | 14:06 | 09:53 | - | 09:54 | 14:12 | - | 12:06 | 15:26 |
| Transects [#] | 5 | 4 | 3 | 5 | 3 | 4 | 3 | 3 | - | 5 | 5 | - | 5 | 5 |
| Q_{CoV} [%] | 1.88 | 3.07 | 3.74 | 4.18 | 3.46 | 2.30 | 2.44 | 2.16 | - | 1.95 | 1.69 | - | 2.42 | 2.03 |
| Q_{tot} [m³/s] | 6217.8 | 6352.0 | 6144.0 | 6010.3 | 6020.0 | 5703.7 | 5406.0 | 4041.6 | - | 3994.6 | 3934.3 | - | 3721.7 | 3652.3 |
| $u_{Q_{tot}}$ [m³/s] | 235.0 | 362.7 | 599.0 | 360.0 | 547.8 | 269.2 | 364.9 | 251.4 | - | 153.8 | 144.0 | - | 157.4 | 142.4 |
| $u_{Q_{tot}}$ [%] | 3.78 | 5.71 | 9.75 | 5.99 | 9.10 | 4.72 | 6.75 | 6.22 | - | 3.85 | 3.66 | - | 4.23 | 3.90 |
| Location | <u>PK</u> | | | | | | | | | | | | | |
| Time | - | 09:14 | 14:04 | 09:45 | 13:49 | 09:15 | 13:23 | 09:23 | 13:10 | 09:11 | 13:34 | 09:25 | 11:30 | 14:42 |
| Transects [#] | - | 3 | 3 | 3 | 4 | 3 | 3 | 4 | 5 | 5 | 5 | 5 | 5 | 5 |
| Q_{CoV} [%] | - | 1.42 | 0.94 | 2.83 | 3.00 | 3.80 | 2.97 | 3.29 | 1.47 | 6.07 | 6.31 | 6.94 | 3.19 | 4.78 |
| Q_{tot} [m³/s] | - | 3209.7 | 3239.6 | 3163.0 | 3100.9 | 2645.9 | 2774.2 | 1964.4 | 1935.6 | 1856.6 | 1774.6 | 1699.4 | 1706.1 | 1783.2 |
| $u_{Q_{tot}}$ [m³/s] | - | 148.0 | 122.1 | 242.0 | 174.9 | 261.9 | 220.8 | 120.2 | 72.4 | 151.1 | 150.0 | 156.3 | 88.2 | 119.7 |
| $u_{Q_{tot}}$ [%] | - | 4.61 | 3.77 | 7.65 | 5.64 | 9.90 | 7.96 | 6.12 | 3.74 | 8.14 | 8.45 | 9.20 | 5.17 | 6.71 |

Uncertainty for each discharge component

The influence of the uncertainty in the different discharge components on the overall uncertainty was analysed and is shown in Figure 15. Figure 15 shows that the pattern between the different discharge components is fairly consistent for all three river branches, except for a few outliers. The absolute uncertainty for each discharge component is a representation of its influence on the overall uncertainty. The absolute uncertainty is largest for the measured discharge in the main channel, because its discharge was responsible for a large fraction of the total discharge, despite having the smallest degree of uncertainty as it was computed directly from the ADCP measurements. The degree of uncertainty for each discharge component is expressed as the ratio of the absolute uncertainty to its mean discharge. After the measured discharge, the estimated top and bottom discharges are responsible for the second and third largest fraction of the total discharge but also have the second and third smallest degree of uncertainty. Therefore, the uncertainty of fully inundated floodplains has a greater influence on the overall uncertainty. Although surrounded by uncertainty, the edge discharges generally have a small influence on the overall uncertainty due to their small fraction of the total discharge.

The outliers in the degree of uncertainty for the floodplains on the right side of Figure 15 are due to negligibly small discharges (i.e., almost equal to zero), thus having a negligible influence on the uncertainty of the total discharge.



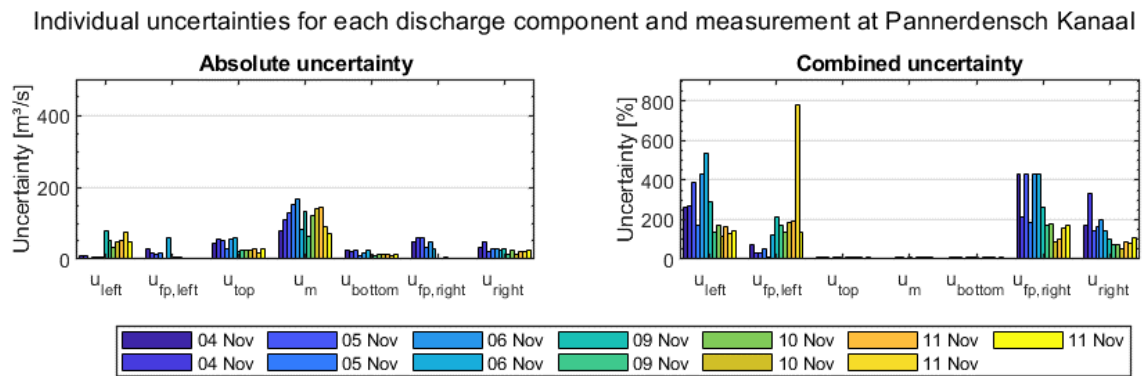


Figure 15: Absolute and combined uncertainties for each discharge component and measurement at the three river branches, the combined uncertainties of components are expressed as percentage of their mean discharges.

Figure 16 shows the uncertainties of all discharge components as a function of the total discharge. It is important to note that the relative uncertainties on the right side of the figure are expressed as a percentage of the total discharge. Furthermore, a linear least-squares line was fitted through the points to better visualise the relationship between uncertainty and total discharge.

The uncertainty of the total discharge (i.e., overall uncertainty) and the measured discharge generally increased as the total discharge increased, for each river branch (left side of Figure 16). In a sense, this phenomenon applied to almost all discharge components (except for the left edge discharge of the Waal), but with a less pronounced increase. Note the differences in the increase of the uncertainties in terms of the absolute value between the river branches because the y-axes have different scales.

In contrast to the absolute uncertainties, the relative uncertainties are actually almost constant over the total discharge of the Bovenrijn, except for the left floodplain (right side of Figure 16). The uncertainty of the left floodplain discharge increases both in absolute and relative terms as the total discharge increases, due to a relatively high discharge during high discharge events combined with a high degree of uncertainty. The uncertainties of the Waal increase in both absolute and relative terms based on the least-squares line in Figure 16, but this gives a distorted picture as there is a strong fluctuation in the points due to the differences in the number of transects as discussed previously (see Table 7).

The Pannerdensch Kanaal is the only one of the three locations where the relative uncertainties decrease as the total discharge increases, except for the floodplains. This pattern is not distorted by the number of transects as there appears to be no correlation with the overall uncertainty (Figure 21). However, the influence of the coefficients of variation plays a role in this (see Table 7), which is relatively low at high discharges since little temporal variation in flow conditions and instrument noise is observed during these measurements. This has also been discussed in section Individual uncertainty sources.

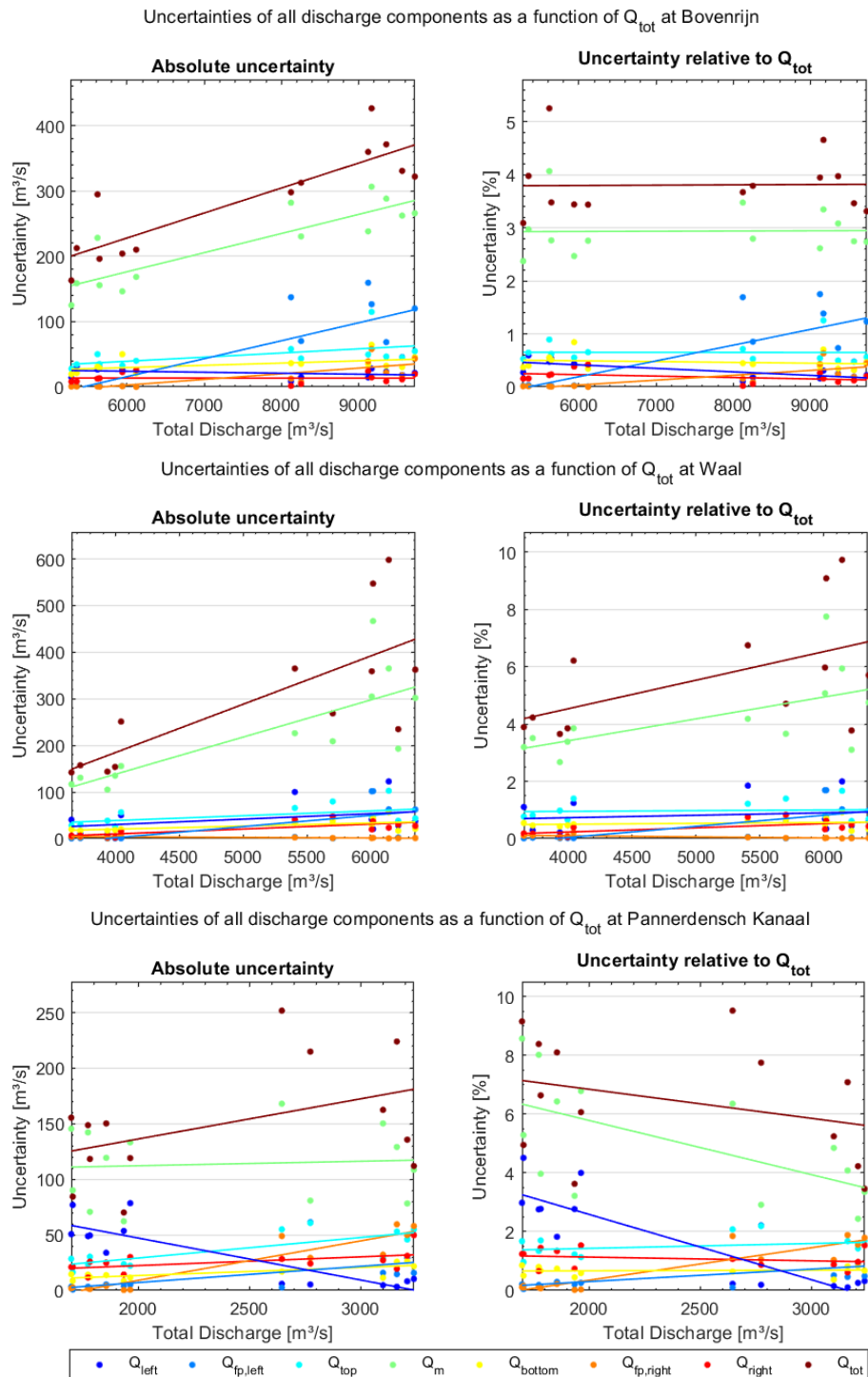


Figure 16: Uncertainties of all discharge components as a function of the total discharge of each measurement and location: the Bovenrijn (upper), the Waal (centre) and the Pannerdensch Kanaal (bottom).

4.2 The uncertainty of the total discharges in the branches and the water balance of the Pannerdensche Kop

Figure 17 shows the mean total discharges estimated from the ADCP flow measurements together with the overall uncertainty at a 95% confidence level represented as an error bar. In addition, the available continuous derived discharges from the period 3 to 11 November 1998 from the nearest discharge stations are plotted. These historical continuous discharges were derived from the operational rating curves of that period.

All continuous derived discharges at Lobith are within the 95% confidence intervals of the estimated ADCP discharges in the Bovenrijn. At two ADCP measurements in the Waal, in the morning and in the afternoon on 10 November 1998, the continuous derived discharge at the Pannerdensche Kop is outside the lower 95% confidence limits of the two estimated ADCP discharges (Figure 17). This suggests that the derived discharge in the Waal at the Pannerdensche Kop was lower than the discharge estimated from the ADCP measurements further downstream at that specific time, which can be partly explained by the time delay of the discharge between the upstream station and the downstream ADCP measurement location in the Waal. Furthermore, these two measurements have the largest number of transects and two of the lowest three estimated uncertainties of all measurements in the Waal (see Table 7) and thus relatively narrow confidence intervals. At three other ADCP measurements in the Waal (i.e., the first and the last two), the continuous derived discharge is close to the lower 95% confidence limits. The highest absolute uncertainties were observed at the discharge peak on 4 November and slightly after.

For one measurement in the Pannerdensch Kanaal, in the afternoon on 9 November, the continuous derived discharge at Pannerden is outside the upper 95% confidence limit. This implies that the historical derived discharge at Pannerden is higher than the discharge estimated from the ADCP measurements at that specific time. However, the station at Pannerden is located further downstream of the ADCP measurement location, so the time delay in the discharge may partly explain this. Moreover, this is the measurement with the lowest overall uncertainty of all measurements in the Pannerdensch Kanaal, both in absolute and relative terms, and hence has the narrowest confidence interval. The lowest overall uncertainty is caused by having the lowest random uncertainty (Figure 14), which is due to having the largest number of transects rather than the coefficient of variation as it is not among the lowest two of all measurements.

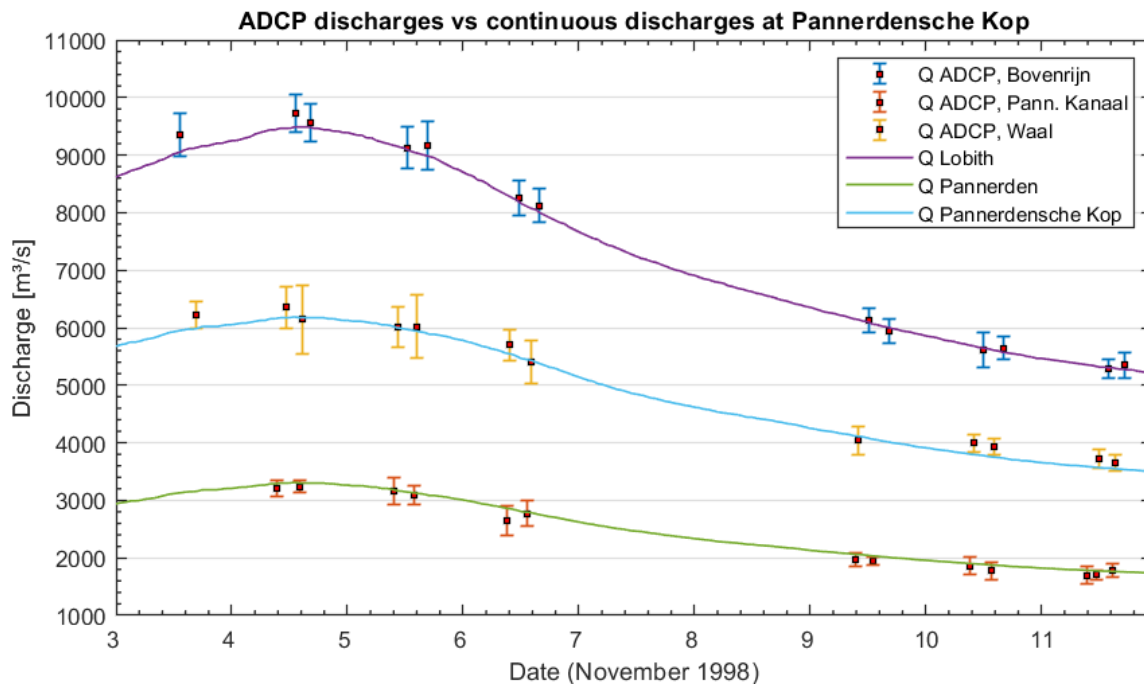


Figure 17: Computed ADCP discharges for each measurement and river branch together with the derived continuous discharges from the same period at the nearest discharge stations (source: <https://waterinfo.rws.nl/>). Figure 18 shows the water balance error including propagated uncertainties (at 95% confidence level) at the Pannerdensche Kop as a function of the upstream discharge in the Bovenrijn. Only same-day ADCP discharge measurements (measurements with at least one measurement in each river branch performed at the same day) were used. This means that the discharge in the Bovenrijn and the Waal on 3 November 1998 is not included, since no measurement is available in the Pannerdensche Kanaal on that day. It can be observed that by including the uncertainties in the river branches, the perfect water balance closure (i.e., WBE is equal to zero) falls within the 95% confidence interval.

It should be noted that the daily averaged ADCP discharges often contain only two measurements and therefore the assumption that the possible water balance errors due to the time delay between the measurement locations have been eliminated is not perfectly valid. The positive water balance error reflects a higher upstream water volume, which may mean that the Bovenrijn discharge is overestimated or that the discharge in either one or both downstream branches is underestimated.

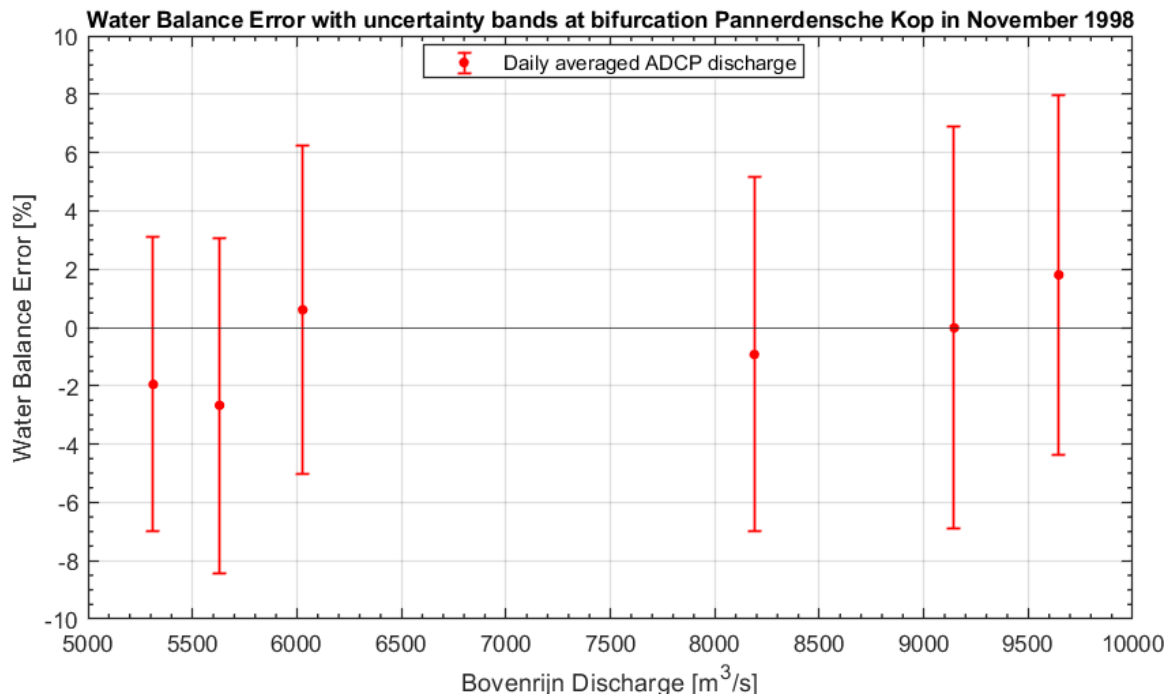


Figure 18: The water balance error including propagated uncertainties at the Pannerdensche Kop for the periods 4-6 and 9-11 November 1998 as a function of the upstream discharge in the Bovenrijn based on the daily averaged ADCP discharges.

5 Discussion

5.1 Uncertainty propagation approach

The uncertainty analysis in this research is based on the QRev software, which is a simplistic approach that combines the uncertainty based on assumptions and what are likely the largest error sources (*QRev – Technical Manual, 2021*). Furthermore, the systematic uncertainty has been estimated based on the standard assumption of QRev and an extensive case study by Huang (2018b). The estimated systematic uncertainty is of the same order of magnitude as assumed in other research studies, including Despax et al. (2019). The different input elemental uncertainties of the systematic uncertainty are normally obtained from experiments (on-site or in laboratory facilities) or from numerical simulations. First, required data for estimating the input elemental uncertainties is not available and second, the ADCP measurements were performed in 1998 so on-site experiments are representative as the conditions at the measurement locations have changed significantly. Furthermore, although the approach is simplistic, QRev is the only method from the mentioned uncertainty propagation methods that is part of routine procedures in U.S. Geological Survey and other hydrometric agencies around the world (Hauet, 2020).

5.2 ADCP error velocity

The ADCP error velocity is the difference between two vertical velocity components of two pairs of opposing acoustic beams (TRDI, 2007). In homogeneous flows, the standard deviation of the error velocity is an indication of the standard deviation due to random error induced by instrument noise and/or low-frequency turbulence at the measuring location (J. A. González-Castro & Muste, 2007). Therefore, a small sensitivity analysis was performed in which the standard deviation of the error velocity was varied by plus minus the water velocity to analyse the influence on the total discharge. A similar approach has also been performed by Moore et al. (2017), only by using a Monte Carlo simulation. In the provided dataset the mean of the error velocity is almost equal to zero, which means that there is a horizontally homogeneous flow. The outcome of the sensitivity analysis showed a significant influence of the error velocity on the total discharge, around 9% difference on average. This meant that the total uncertainty was mainly determined by the error velocity, so it has been decided not to include this in the uncertainty analysis of the total discharge. This is supported by the fact that the random error is already included by taking the standard deviation over multiple transects and in other uncertainty propagation methods for moving-boat ADCP measurements the error velocity is also not included (Despax et al., 2019; García et al., 2012; J. A. González-Castro & Muste, 2007; Huang, 2018a). The QRev software also does not include the ADCP error velocity directly in the uncertainty analysis, there it only serves as a quality indicator for determining invalid data in the pre-processing stage (*QRev – Technical Manual, 2021*).

5.3 Flow inhomogeneity

Turbulence-induced spatial variations affect the quality of velocity estimates by introducing flow inhomogeneity. Other sources of inhomogeneity include mixing layers at confluences, which is the case at the Bovenrijn near Lobith due to the Griethauser Altrhein. The ADCP flow measurements in the provided dataset from 1998 generally contain little transects for each measurement. A correlation analysis has been performed and showed that there was a clear negative correlation between the number of transects and the uncertainty in the total discharge for the Waal (Figure 21, Appendix C) and it is known that a higher number of successive transects is important for reducing the uncertainty in ADCP measurements (Oberger & Mueller, 2007). However, the correlation analysis was performed

with a small number of measurements, but still this gives a distorted picture, as the largest uncertainties are probably overestimated compared to the lowest uncertainties.

5.4 Uncertainty in floodplain discharges

It is important to note that the differences in uncertainties between the various discharge components also strongly depend on how the discharge components are defined. The measured discharge (Q_m), top discharge (Q_{top}) and the bottom discharge (Q_{bottom}) are enclosed in the main channel bounded by fixed embankments. Although this does not make much difference for these discharge components, it does for the floodplain and edge discharges. All ADCP flow measurements showed that the measuring boat, crossing from one bank to another, travelled a greater distance closer to the bank where it started. As a result, the measured portion between the left and right floodplains differs strongly between the reciprocal transects. If the boat started navigating at the right bank, the measured portion of the right floodplain is larger than when it ended at the right bank and vice versa. This appears to be the main reason for the high uncertainties in the floodplain discharges from these results, as the standard deviation of the floodplain discharge is high and so was the random uncertainty. To determine the total discharge, however, this was compensated for with the left and right edge discharge, since the edge distance was greater where the boat ended and vice versa. However, purely looking at the uncertainties in the edge discharges and floodplain discharges, this gives a distorted picture because the floodplain and edge discharges were strongly correlated to each other.

This makes it difficult to independently analyse the uncertainty of floodplains. One possibility would be to merge the opposing edges and floodplains, but still a difference remained. Separating the floodplains from the main channel has, however, ensured that the velocity profile of the floodplains can be determined more accurately since the hydrodynamic conditions differ from the main channel.

6 Conclusion

6.1 Uncertainties in high river discharge measurements and their weight on the overall uncertainty

The first research question aims to identify the uncertainties introduced in high river discharge measurements and to quantify the weight of each uncertainty on the uncertainty of the total discharge (i.e., overall uncertainty). The overall uncertainty is subdivided into individual uncertainty sources consisting of the random uncertainty, edge uncertainty, extrapolation uncertainty, velocity accuracy uncertainty, bottom depth accuracy uncertainty and systematic uncertainty. The random uncertainty and systematic uncertainty have the most influence on the overall uncertainty. The systematic uncertainty is assumed constant for each measurement with a 95% confidence interval of 2.94% of the total discharge, while the random uncertainty depends on the coefficient of variation of the total discharge for all transects and the number of transects. The uncertainty due to extrapolation only plays a minor role in the Pannerdensch Kanaal when the floodplains are inundated but no ADCP measurements have been performed. This is because the Pannerdensch Kanaal has the smallest total discharges, so the extrapolated floodplain discharges have a slightly greater influence on the overall uncertainty. The uncertainty due to the estimated edge discharge, ADCP velocity accuracy and bottom depth accuracy have proven to be negligible under the current circumstances. This is explained by the small fraction of the edge discharge relative to the total discharge and the relatively high accuracy of the ADCP instrument, also because of relatively high flow velocities.

In addition, the uncertainty was also estimated for all discharge components individually, i.e., the left edge discharge, the left floodplain discharge, the top discharge, the measured discharge, the bottom discharge, the right floodplain discharge and the right edge discharge. This provides insight into the contribution of the uncertainty of each discharge component to the uncertainty of the total discharge. The pattern between the different discharge components is fairly consistent for all three river branches, except for a few outliers. Although the measured discharge in the main channel has the lowest degree of uncertainty because it is computed directly from the ADCP measurements, it has the greatest influence on the overall uncertainty as its discharge is responsible for a large fraction of the total discharge. After the measured discharge, the top and bottom discharges account for the second and third largest fraction of the total discharge but also have the second and third smallest degree of uncertainty. As a result, the fully inundated floodplains have a larger influence on the overall uncertainty. Although surrounded by uncertainty, the edge discharges generally have a small influence on the overall uncertainty due to their small fraction of the total discharge.

However, the uncertainties in the edge and floodplain discharges are highly dependent on which side the measuring boat starts measuring. The measured portion between the left and right floodplains differs strongly between the reciprocal transects and this appears to be the main reason for the large uncertainties in the floodplain discharges in this research. This makes it difficult to independently outline the uncertainty of floodplain discharges and its influence on the overall uncertainty.

6.2 The uncertainty of the total discharges in the branches and the water balance of the Pannerdensche Kop

The second research question aims to determine which river branch has the largest overall uncertainty and most likely causes the water balance error at the Pannerdensche Kop bifurcation. First, the three river branches at the Pannerdensche Kop were compared in terms of the overall uncertainty. The overall uncertainties in the Bovenrijn are fairly constant over all measurements, ranging from 3.09% to 5.25%.

In the Waal, there are larger fluctuations in the overall uncertainty over time (i.e., from 3.66% to 9.75%), where the largest uncertainties are observed at the discharge peak and slightly after. However, a conducted correlation analysis showed that both the overall uncertainty and the coefficient of variation of the total discharge in the Waal are negatively correlated with the number of transects. This gives a distorted picture, as the largest uncertainties are probably overestimated compared to the lowest uncertainties. Under the conditions in the Waal at that time, the natural turbulence and instrument noise had a great influence on the overall uncertainty, which could have been reduced by a higher number of successive transects. This is in contrast to the Bovenrijn and the Pannerdensch Kanaal, where there appears to be no correlation between the overall uncertainty and the number of transects, so a higher number of transects would not have led to a lower uncertainty of the total discharge.

The Pannerdensch Kanaal is characterised by relatively large uncertainties over time, ranging from 3.74% to 9.90%. Most of the large uncertainties are observed at lower discharges and this is explained by higher coefficients of variation of the total discharge possibly caused by random error, temporal variation in flow conditions or instrument noise.

Finally, the comparison between the estimated ADCP discharges and the historical discharges derived from the rating curves for each river branch showed that there is no systematic over- or underestimation of the discharge by the rating curves for any of the branches. However, two ADCP measurements in the Waal and one in the Pannerdensch Kanaal are respectively under- and overestimated by the rating curve, but this can partly be explained by the time delay in the discharge between the discharge station and the ADCP measurement location. Additionally, it was found that by including the uncertainties in the river branches into the water balance error, the perfect water balance closure falls within the 95% confidence interval for all same-day ADCP measurements in the three branches. Therefore, the water balance error at the Pannerdensche Kop can be explained by the uncertainties in the three river branches and there seems to be no river branch that most likely caused the water balance error.

7 Recommendations

Based on the findings in this research, a number of recommendations are made for possible future research.

Due to the negative correlation between the overall uncertainty and the number of transects for the Waal, it is recommended to use a dataset with a larger number of transects for all ADCP measurements for future research to find out whether there might be a river branch most likely to cause the water balance error at the Pannerdensche Kop.

Furthermore, it is recommended to further investigate the uncertainties of the discharge in fully inundated floodplains as these appeared to have a larger influence on the overall uncertainty than the estimated uncertainty of the top and bottom discharge for almost every river branch. For example, a WAQUA model could be used to simulate the hydrodynamic flows over the floodplains to get a better understanding of possible uncertainties in the floodplain discharges from a 2DH perspective.

Finally, it is recommended to analyse the uncertainties in the high discharge measurements of more recent datasets, as there have been spatial changes and changes in flow conditions around the Pannerdensche Kop.

References

- Berends, K. (2019). *Human intervention in rivers: quantifying the uncertainty of hydraulic model predictions* [University of Twente]. <https://doi.org/1.9789036548823>
- Brand, G. (2011). *Debietmeten in extreme situaties, inventarisatie intern RWS*. Rijkswaterstaat, Ministerie van Infrastructuur en Milieu.
- Buschman, F., Blom, A., van Dijk, T., Kleinhans, M. G., & van der Mark, C. F. (2017). *Informatiebehoefte en aanbevelingen voor monitoring in de Bovendelta van de Rijn*. Deltares.
- Despax, A., Le Coz, J., Hauet, A., Mueller, D. S., Engel, F. L., Blanquart, B., Renard, B., & Oberg, K. A. (2019). Decomposition of Uncertainty Sources in Acoustic Doppler Current Profiler Streamflow Measurements Using Repeated Measures Experiments. *Water Resources Research*, 55(9), 7520–7540. <https://doi.org/10.1029/2019WR025296>
- Eij, J. M. (2004). Verwerking van ADCP stromingsmetingen rond de Pannerdensche Kop tijdens hoogwater in november 1998. In *Technical Report AV DOC 040211*.
- García, C. M., Tarrab, L., Oberg, K., Szupiany, R., & Cantero, M. I. (2012). Variance of Discharge Estimates Sampled Using Acoustic Doppler Current Profilers from Moving Platforms. *Journal of Hydraulic Engineering*, 138(8), 684–694. [https://doi.org/10.1061/\(asce\)hy.1943-7900.0000558](https://doi.org/10.1061/(asce)hy.1943-7900.0000558)
- Gensen, M. R. A. (2021). *Discharge and water level uncertainty in bifurcating rivers* [University of Twente]. <https://doi.org/10.3990/1.9789036553056>
- Gensen, M. R. A., Warmink, J. J., Berends, K. D., & Huthoff, F. (2021). *Improving rating curve accuracy by incorporating water balance closure at river bifurcations*. University of Twente.
- González-Castro, J. A., & Muste, M. (2007). Framework for Estimating Uncertainty of ADCP Measurements from a Moving Boat by Standardized Uncertainty Analysis. *Journal of Hydraulic Engineering*, 133, 1390–1410. [https://doi.org/10.1061/\(ASCE\)0733-9429\(2007\)133](https://doi.org/10.1061/(ASCE)0733-9429(2007)133)
- González-Castro, J., Buzard, J., & Mohamed, A. (2016). RiverFlowUA—A package to estimate total uncertainty in ADCP discharge measurements by FOTSE—with an application in hydrometry,. *River Flow 2016*, 715–723.
- Hartong, H., & Termes, P. (2009). *Handboek debietmeten in open waterlopen*. (Issue 41). STOWA. <http://agris.fao.org/agris-search/search.do?recordID=NL2012045275>
- Hauet, A. C. (2020). *Uncertainty of discharge measurement methods : a literature review*.
- Huang, H. (2017). Why Moving-Boat Adcp Streamflow Measurement Does Not Require a Straight-Line Path. *Proceedings of the 37th IAHR World Congress*, 6865(1), 5433–5438.
- Huang, H. (2018a). A modified Simpson model for estimating random uncertainty of moving-boat ADCP streamflow measurements. *Flow Measurement and Instrumentation*, 61(December 2017), 84–93. <https://doi.org/10.1016/j.flowmeasinst.2018.03.002>
- Huang, H. (2018b). Estimating Bias Limit of Moving-Boat ADCP Streamflow Measurements. *Journal of Hydraulic Engineering*, 144(6), 04018024. [https://doi.org/10.1061/\(asce\)hy.1943-7900.0001465](https://doi.org/10.1061/(asce)hy.1943-7900.0001465)
- Jain, S. K., & Singh, V. P. (2003). Chapter 2 - Acquisition and Processing of Water Resources Data. *Developments in Water Science*, 51(C), 47–121. [https://doi.org/10.1016/S0167-5648\(03\)80056-4](https://doi.org/10.1016/S0167-5648(03)80056-4)
- JCGM. (2008). Evaluation of measurement data — Guide to the expression of uncertainty in

- measurement. In *BIPM* (Vol. 1, Issue 100).
- Moore, S. A., Jamieson, E. C., Rainville, F., Rennie, C. D., & Mueller, D. S. (2017). Monte Carlo Approach for Uncertainty Analysis of Acoustic Doppler Current Profiler Discharge Measurement by Moving Boat. *Journal of Hydraulic Engineering*, 143(3), 04016088. [https://doi.org/10.1061/\(asce\)hy.1943-7900.0001249](https://doi.org/10.1061/(asce)hy.1943-7900.0001249)
- Mueller, D. S. (2013). Extrap: Software to assist the selection of extrapolation methods for moving-boat ADCP streamflow measurements. *Computers and Geosciences*, 54, 211–218. <https://doi.org/10.1016/j.cageo.2013.02.001>
- Mueller, D. S. (2016). QRev - software for computation and quality assurance of acoustic Doppler current profiler moving-boat streamflow measurements - user's manual for Version 2.8. *U.S. Geological Survey Open-File Report 2016-1052, March*, 50.
- Mueller, D. S., & Wagner, C. R. (2009). Measuring Discharge with Acoustic Doppler Current Profilers from a Moving Boat. In *U.S. Geological Survey Techniques and Methods 3A-22* (p. 72). <http://pubs.water.usgs.gov/tm3a22>
- Oberg, K., & Mueller, D. (2007). Validation of streamflow measurements made with acoustic Doppler current profilers. *Journal of Hydraulic Engineering*, 133(12). [https://doi.org/10.1061/\(ASCE\)0733-9429\(2007\)133:12\(1421\)](https://doi.org/10.1061/(ASCE)0733-9429(2007)133:12(1421))
- Pierrefeu, G., Berthet, T., Le Boursicaud, R., Bompard, P., Triol, T., & Blanquart, B. (2017). OURSIN: Uncertainty distribution tool for moving-boat ADCP measurements. *SHF, Colloque Hydrométrie 2017*, 17.
- QRev — Technical Manual*. (2021).
- Quartel, S., van der Veen, R., Wijbenga, A., Berben, F., Kok, F., & Heinen, P. (2011). Dynamic stage-discharge relations of the Dutch Rhine branches. *Abstract in NCR Days 2011: Controlling the Dutch Rivers*, 35–36.
- Rijkswaterstaat Oost-Nederland. (2000). *Verlaging Millingse dam Projectnota*.
- Rijkswaterstaat Water Verkeer en Leefomgeving. (2019). *Rivierkundig beoordelingskader voor ingrepen in de Grote Rivieren*. Rijkswaterstaat Water, Verkeer en Leefomgeving.
- Staatsbosbeheer. (2022). *Herinrichting Millingerwaard: Werk in uitvoering*. Staatsbosbeheer. <https://millingerswaard.staatsbosbeheer.nl/werk+in+uitvoering/default.aspx>
- TRDI. (2007). *WorkHorse: Monitor, Sentinel, Mariner ADCP (Technical manual)*. Teledyne RD Instruments.
- TRDI. (2016). *WinRiver II: Software User's Guide* (Issue August). Teledyne RD Instruments.
- Twijnstra, J. J., Gensen, M. R. A., Warmink, J. J., Hulscher, S. J. M. H., Huthoff, F., & Horn, G. (2020). MSc thesis: Water balance in the Dutch river Rhine and uncertainty of rating curves. *Abstract from NCR Days 2020: Managing Changing Rivers*, 84–85.
- Van Velzen, E. H., Jesse, P., Cornelissen, P., & Coops, H. (2003). *Stromingsweerstand vegetatie in uiterwaarden*. Rijksinstituut voor Integraal Zoetwaterbeheer en Afvalwaterbehandeling.
- Vermeulen, B., Ribberink, J. S., de Vriend, H. J., Hulscher, S. J. M. H., & Souren, A. W. M. G. (2019). *River flow and sediment transport lecture notes*. https://canvas.utwente.nl/courses/5153/files/1384963?module_item_id=135959
- Visser, M., & Klopstra, D. (2002). *Onderzoek nauwkeurigheid debietrandvoorwaarden Noordelijk Deltabekken*. Rijkswaterstaat Directie Zuid-Holland.

Appendix A: Equations of extrapolation methods

The following equations are used to estimate the uncertainty in the selected extrapolation method.

Constant extrapolation method (Mueller & Wagner, 2009):

$$Q_{top} = \sum_{j=1}^{Ensembles} V_{1,j} \cdot (z_{ws} - z_{tb}) \cdot W \quad (20)$$

Where,

- $V_{1,j}$ = water velocity in topmost measured depth-cell [m/s]
- $z_{ws,j}$ = distance from the bed to the water surface [m]
- $z_{tb,j}$ = distance from the bed to the top of the topmost depth-cell [m]
- W_j = width of ensemble [m]

3-point slope fit extrapolation (Mueller & Wagner, 2009):

$$Q_{top} = \sum_{j=1}^{Ensembles} \left(\frac{A_j}{2} \cdot (z_{ws} - z_{tb})^2 + B_j \cdot (z_{ws} - z_{tb}) \right) \cdot W \quad (21)$$

Where,

- A_j = slope of the three topmost measured depth-cells [1/s]
- B_j = V -intercept [m/s]
- z_{ws} = distance from the bed to the water surface [m]
- z_{tb} = distance from the bed to the top of the topmost depth-cell [m]
- W = width of ensemble [m]

Appendix B: Figures

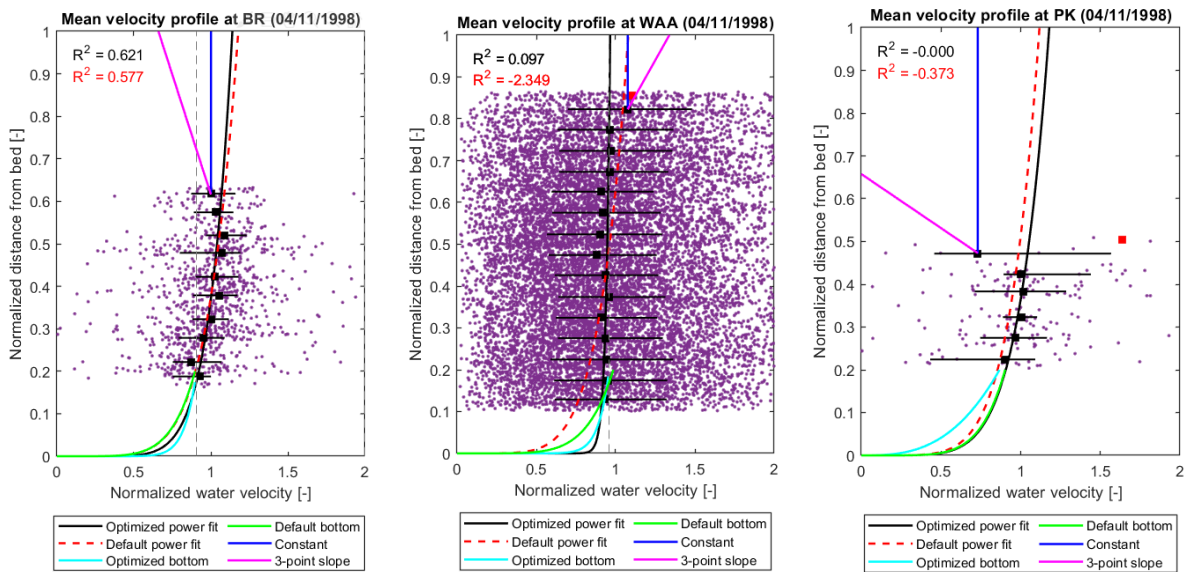


Figure 19: Three plots of normalised data in the floodplains showing cloud of points from depth-cells (purple dots), median values for each 5%-increment (black squares), interquartile range for each increment (black whiskers), and the possible extrapolation methods. Left: for the Bovenrijn (BR). Centre: for the Waal (WAA). Right: for the Pannerdensch Kanaal (PK).

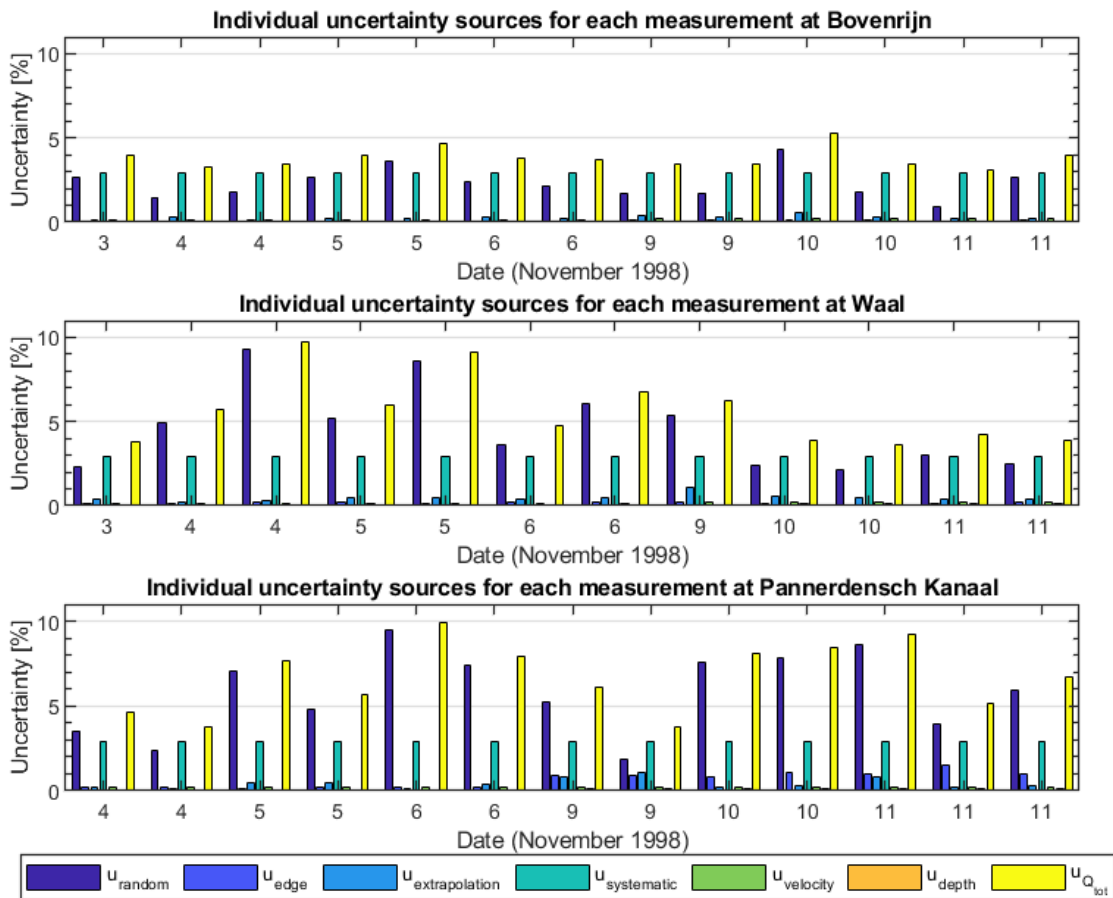


Figure 20: Individual uncertainty sources (at 95% confidence level) over time for the three river branches, with relative values in percentage of total discharge.

Appendix C: Correlation analysis

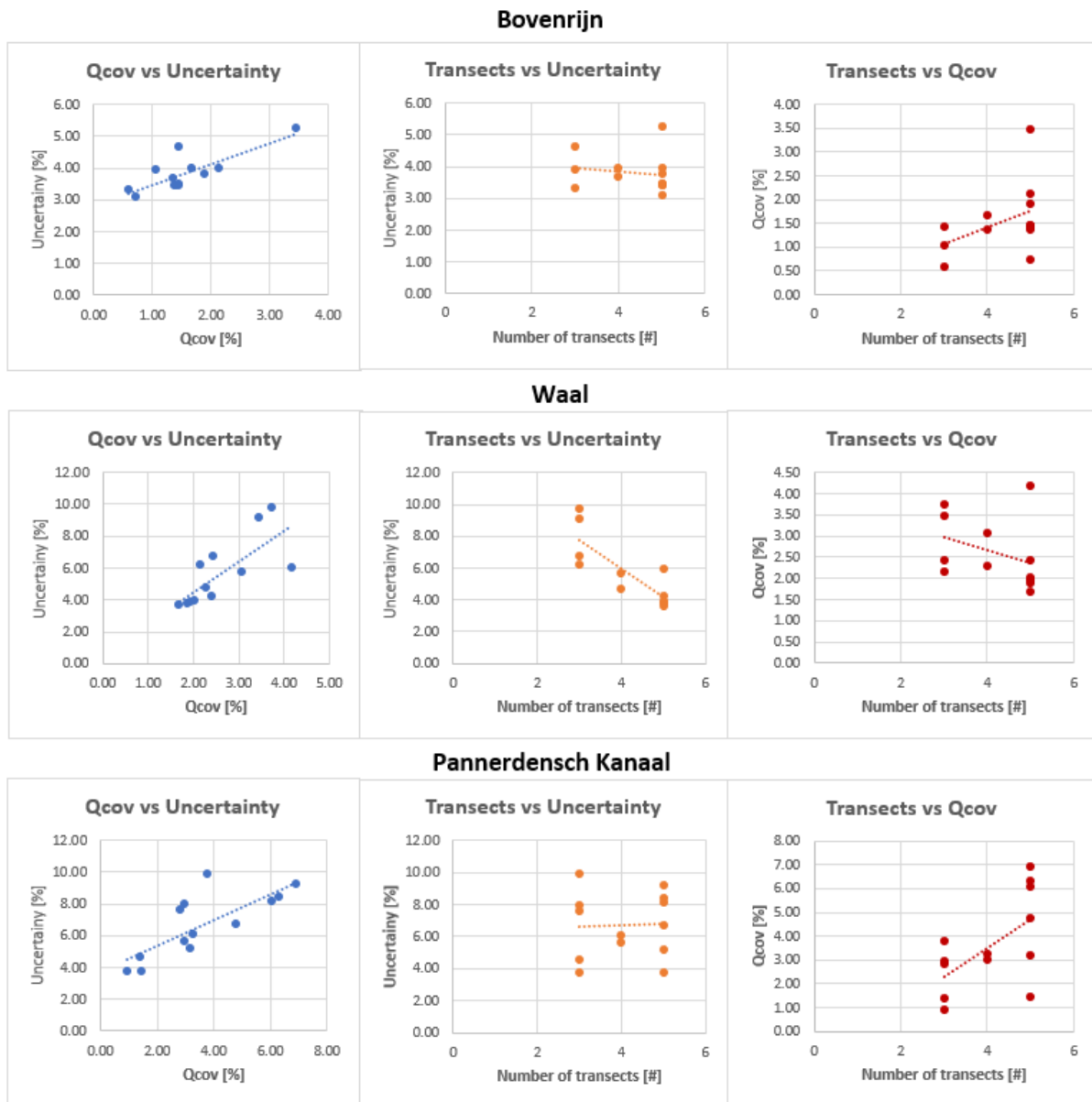


Figure 21: Correlation analysis of the variables: Q_{Cov} , number of transects and the overall uncertainty.